Version of Record at: https://doi.org/10.1029/2023JG007404

Check for updates

JGR Biogeosciences

RESEARCH ARTICLE
10.1029/2023JG007404

Key Points:

- Physiochemical mechanisms control horizontal exchange of carbon across marsh-tidal channel interfaces, affecting lateral carbon flux
- Dissolution and reprecipitation of carbon-bearing Fe oxides during flood and ebb tides control the horizontal mobility of carbon
- Hydraulic gradients control the carbon character in the tidal channel, and rising tides push greenhouse gases out of the channel bank

Supporting Information:

Supporting Information may be found in the online version of this article.

Correspondence to:

A. L. Seyfferth,
angelias@udel.edu

Citation:

Fettrow, S., Jeppi, V., Wozniak, A., Vargas, R., Michael, H., & Seyfferth, A. L. (2023). Physiochemical controls on the horizontal exchange of blue carbon across the salt marsh-tidal channel interface. *Journal of Geophysical Research: Biogeosciences*, *128*, e2023JG007404. https://doi.org/10.1029/2023JG007404

Received 20 JAN 2023
Accepted 17 MAY 2023

Author Contributions:

Conceptualization: Sean Fettrow, Virginia Jeppi, Andrew Wozniak, Rodrigo Vargas, Holly Michael, Angelia L. Seyfferth
Formal analysis: Sean Fettrow
Funding acquisition: Holly Michael, Angelia L. Seyfferth
Investigation: Sean Fettrow, Virginia Jeppi
Methodology: Sean Fettrow, Andrew Wozniak, Rodrigo Vargas, Angelia L. Seyfferth
Project Administration: Angelia L. Seyfferth
Resources: Andrew Wozniak, Rodrigo Vargas, Holly Michael, Angelia L. Seyfferth
Supervision: Angelia L. Seyfferth

© 2023. American Geophysical Union. All Rights Reserved.

Physiochemical Controls on the Horizontal Exchange of Blue Carbon Across the Salt Marsh-Tidal Channel Interface

Sean Fettrow[1], Virginia Jeppi[1], Andrew Wozniak[2], Rodrigo Vargas[1], Holly Michael[3,4], and Angelia L. Seyfferth[1]

[1]Department of Plant and Soil Sciences, University of Delaware, Newark, DE, USA, [2]School of Marine Science and Policy, University of Delaware, Lewes, DE, USA, [3]Department of Earth Sciences, University of Delaware, Newark, DE, USA, [4]Department of Civil and Environmental Engineering, University of Delaware, Newark, DE, USA

Abstract Tidal channels are biogeochemical hotspots that horizontally exchange carbon (C) with marsh platforms, but the physiochemical drivers controlling these dynamics are poorly understood. We hypothesized that C-bearing iron (Fe) oxides precipitate and immobilize dissolved organic carbon (DOC) during ebb tide as the soils oxygenate, and dissolve into the porewater during flood tide, promoting transport to the channel. The hydraulic gradient physically controls how these solutes are horizontally exchanged across the marsh platform-tidal channel interface; we hypothesized that this gradient alters the concentration and source of C being exchanged. We further hypothesized that trace soil gases (i.e., CO_2, CH_4, dimethyl sulfide) are pushed out of the channel bank as the groundwater rises. To test these hypotheses, we measured porewater, surface water, and soil trace gases over two 24-hr monitoring campaigns (i.e., summer and spring) in a mesohaline tidal marsh. We found that Fe^{2+} and DOC were positively related during flood tide but not during ebb tide in spring when soils were more oxidized. This finding shows evidence for the formation and dissolution of C-bearing Fe oxides across a tidal cycle. In addition, the tidal channel contained significantly ($p < 0.05$) more terrestrial-like DOC when the hydraulic gradient was driving flow toward the channel. In comparison, the channel water was saltier and contained significantly ($p < 0.05$) more marine-like DOC when the hydraulic gradient reversed direction. Trace gas fluxes increased with rising groundwater levels, particularly dimethyl sulfide. These findings suggest multiple physiochemical mechanisms controlling the horizontal exchange of C at the marsh platform-tidal channel interface.

Plain Language Summary Tidal salt marshes store large amounts of carbon belowground in soils, but there is also a significant amount of carbon flowing into and out of these ecosystems via tidal channels. We investigated the carbon flowing between the channel bank and surface water in a salt marsh in Delaware. We found that soil minerals (i.e., iron oxides) control the mobility of carbon as iron oxides retain carbon during ebb tides and release carbon during flood tides as the minerals dissolve. The gradient between the groundwater and surface water elevation (i.e., hydraulic gradient) controls the flow direction for dissolved carbon, altering the concentration and source of carbon found in the tidal channel across tidal cycles. In addition, gases trapped in channel banks are pushed out of the soils as the tide rises. These findings will improve our understanding of carbon cycles in these critical carbon sinks.

1. Introduction

Tidal salt marshes store so-called "blue carbon" (Nellemann et al., 2009) in high quantities relative to their land area (Chmura et al., 2003; Duarte et al., 2008, 2013) and could be used to mitigate climate change (Howard et al., 2017; IPCC, 2014; Macreadie et al., 2021; Serrano et al., 2019), but we are just beginning to understand C dynamics in these complex ecosystems. Most blue C studies focus on the distribution of C in the soil profile (Berthelin et al., 2022; Chmura et al., 2003; Gorham et al., 2021; Hinson et al., 2017; Spivak et al., 2019; Sun et al., 2019; J. Yu et al., 2014; Van De Broek et al., 2016) or vertical trace gas fluxes (Abdul-Aziz et al., 2018; Capooci et al., 2019; Capooci & Vargas, 2022a; Diefenderfer et al., 2018; O'Connor et al., 2020; Tong et al., 2020; Vázquez-Lule & Vargas, 2021; Wollenberg et al., 2018). Few studies focus on the lateral C flux, which is the inorganic and organic C imported and exported via tidal channels (Santos et al., 2021; Trifunovic et al., 2020). This limited attention has likely led to an underestimation of the net C flux within coastal wetlands. Some studies suggest that lateral C export may be similar to or even exceed blue C burial rates (Bogard et al., 2020; Czapla et al., 2020; Mcleod et al., 2016; Santos et al., 2019; Z. A. Wang et al., 2016). These studies suggest

Version of Record at: https://doi.org/10.1029/2023JG007404

Writing – original draft: Sean Fettrow, Angelia L. Seyfferth
Writing – review & editing: Virginia Jeppi, Andrew Wozniak, Rodrigo Vargas, Holly Michael

the importance of the lateral C flux, but much uncertainty exists as the range in global salt marsh lateral flux is 31–78 Tg C yr^{-1}, and there are limited studies indicating why the range is so large (Duarte, 2017). Further study is required to reduce uncertainty and better understand carbon dynamics in tidal salt marshes.

Although it is increasingly recognized that the lateral C flux may represent a substantial component of the net C budget in tidal wetlands, there remains high uncertainty. The uncertainty of lateral C flux in North American tidal wetlands is 100% of the estimated value (Hayes et al., 2018). This high uncertainty stems from several factors, including (a) few studies examining lateral C transport (Chu et al., 2018; Santos et al., 2019; Z. A. Wang et al., 2016; Z. A. Wang & Cai, 2004), (b) lack of incorporation of both DOC and DIC into estimates (Duarte, 2017; Santos et al., 2019), (c) few studies on lateral trace gas C fluxes from tidal channels (Trifunovic et al., 2020), and (d) limited mechanistic understanding of horizontal C exchange between the salt marsh soil platform and tidal channel interface. For the latter point, most studies focus on large-scale surface water flux between the marsh, estuary, and ocean boundaries (Chu et al., 2018; Najjar et al., 2018; Osburn et al., 2015; Tzortziou et al., 2008; Z. A. Wang & Cai, 2004; Winter et al., 1996), whereas only a few address the horizontal exchange of C-rich porewater between marsh soils and surface water in tidal channels (Guimond, Seyfferth, et al., 2020). Therefore, having an improved mechanistic understanding of the physicochemical controls on horizontal C exchange between the tidal channel and adjacent marsh soil could help decrease uncertainty in the larger-scale lateral C flux.

The chemical mobility of DOC in soils near tidal channels may be controlled by Fe oxides, hydroxides, and oxyhydroxides (hereafter referred to as "Fe oxides"), which offer mineral protection from microbial degradation and decrease the mobility of C (Zak & Gelbrecht, 2007). The role of Fe oxides in stabilizing DOC has been well established in controlled laboratory experiments, and upland terrestrial field settings (Adhikari et al., 2019; Chen & Sparks, 2015; Sowers, Adhikari, et al., 2018; Sowers et al., 2019; Sowers, Stuckey, & Sparks, 2018), but the importance of Fe oxides in coastal settings is less clear. Previous work has shown that reactive Fe oxide phases, including ferrihydrite, are abundant in soils adjacent to tidal salt marsh channels along with high quantities of DOC (Seyfferth et al., 2020). These soils are inundated and drain every 6 hr due to semidiurnal tides, causing rapid and large changes in soil redox potentials over short periods (Guimond, Seyfferth, et al., 2020). Due to the redox sensitivity of Fe oxides (Schwertmann, 1991), reducing and oxidizing conditions in tidally influenced soils may allow coprecipitates of Fe and DOC to form and dissolve between ebb and flood tides, as has been shown for other fluctuating redox environments (Chen et al., 2014; Sodano et al., 2017). Thus, precipitation and dissolution of Fe-DOC coprecipitates across ebb-flood tides may be an important process controlling the transport of marsh soil DOC to and from tidal channels. The presence of Fe-DOC coprecipitates in salt marsh soils has previously been confirmed, as has their sensitivity to redox conditions under simulated sea level rise conditions (Fettrow et al., 2023).

While Fe oxides may partially control the chemical mobility of horizontally transported C, the physical transport of porewater solutes is governed by the hydraulic gradient between the near-channel groundwater and the tidal channel surface water (Guimond, Yu, et al., 2020). The hydraulic gradient likely changes rapidly in semi-diurnal systems, where a falling tide leads to groundwater/porewater discharge into the tidal channel, and a rising tide leads to surface water seepage into the pore space (Xin et al., 2011). Changes in hydraulic gradient direction will likely alter the source and concentration of C being laterally exchanged or lost, such as light-reactive chromophoric dissolved organic carbon (CDOM). The proportion of marsh-derived, terrestrial-like CDOM has been shown to increase in tidal channels during ebb tide, while the proportion of marine-derived CDOM increases during flood tide (Osburn et al., 2015; Tzortziou et al., 2008). This is likely a result of C-rich marsh porewater flowing into the tidal channel during ebb tide and estuarine bay waters flowing into the tidal channel during flood tide. Still, to our knowledge, a direct connection between the magnitude and composition of C in the tidal channel and the horizontal exchange of water between the marsh platform and tidal channel is yet to be made over a complete tidal cycle and across seasons.

In addition to understanding the physical and chemical controls on horizontal C transport, it is also essential to know how soil trace gas emissions change across tidal cycles (Capooci & Vargas, 2022b). Fluxes of soil greenhouse gases (e.g., CO_2, CH_4) offset the global cooling effect of stored C in soil. Therefore, assessing the horizontal fluxes of gases is critical to constraining the total ecosystem C flux (Santos et al., 2019; Trifunovic et al., 2020). In addition to CO_2 and CH_4, dimethyl sulfide (DMS) is a common C-containing gas produced in salt marshes, particularly those dominated by *Spartina* grasses (Capooci & Vargas, 2022b; Wang & Wang, 2017).

Version of Record at: https://doi.org/10.1029/2023JG007404

DMS is a climate-cooling gas due to its oxidation to SO_4 in the atmosphere (Charlson et al., 1987). Few studies have investigated horizontal trace gas fluxes from tidal channels, but evidence suggests these sites could represent biogeochemical hotspots in salt marshes (Trifunovic et al., 2020). Assessing soil trace gas emissions coupled to porewater and surface water near tidal channels may help constrain the magnitude and mechanisms of lateral C fluxes in tidally influenced ecosystems.

We postulated several interrelated hypotheses to investigate patterns and mechanisms of horizontal C flux between the marsh platform and tidal channel. First, we hypothesized that Fe oxides stabilize DOC during high soil redox conditions (i.e., ebb tide), while they dissolve and enter the porewater together as Fe^{2+} and DOC during low soil redox conditions (i.e., flood tide). Second, we hypothesized that the hydraulic gradient controls the physical exchange of solutes between the marsh porewater and the tidal channel and drives changes in the concentration and source (i.e., marine vs. terrestrial) of lateral C. Third, we hypothesized that soil trace gases are horizontally lost (i.e., horizontal fluxes) from channel bank soils to tidal channels due to tidal forces and the upward movement of groundwater. To test these hypotheses, we performed two 24-hr field campaigns of hourly porewater and soil trace gas fluxes during the growing season in a mesohaline temperate salt marsh. We focused on spring tides when water level and soil redox potentials are at extremes, possibly representing the largest exchange across the terrestrial-water interface. Our data highlight how interactions between physiochemical processes control the horizontal flow of C between marsh soils and adjacent tidal channels, with implications for improving our understanding of the lateral C flux between salt marshes and the coastal ocean.

2. Methods and Materials

2.1. Field Site

The samples and measurements were taken from and adjacent to the tidal channel of a temperate salt marsh located at the St Jones Estuarine Research Reserve in Dover, DE (Figure S1 in Supporting Information S1). This field site has been described extensively in previous work (Capooci et al., 2019; Capooci & Vargas, 2022a; Guimond, Seyfferth, et al., 2020; Guimond, Yu, et al., 2020; Seyfferth et al., 2020; Trifunovic et al., 2020). Tidal channel salinity ranges from 8 to 15 parts per thousand (ppt) (Capooci et al., 2019) and flows into the nearby St Jones River that is connected to the Delaware Bay. Vegetation near the tidal channel consists primarily of *Spartina alterniflora*, with patches of both *S. patens* and *S. cynosuroides*. The soils at the sampling location are textured as a silty clay loam (Capooci et al., 2019). The upper 1 m of these soils were previously reported to contain ∼150–300 mmol kg^{-1} ammonium oxalate (AAO)-extractable Fe and ∼10–14 mmol kg^{-1} citrate-bicarbonate-dithionite (CBD)-extractable Fe, representing poorly crystalline and total free Fe, respectively (Seyfferth et al., 2020). These soils contain approximately 4% C and Fe with approximately 40% of the solid-phase Fe present as ferrihydrite and Fe-DOC coprecipitates are also present (Fettrow et al., 2023; Seyfferth et al., 2020). Semidiurnal tides inundate soils near the tidal channel twice daily and drain as the tides go out, causing redox conditions to change drastically (−100 to 500 mV) and rapidly across a single tidal cycle (Guimond, Seyfferth, et al., 2020), particularly during spring tides when the tidal amplitude is at its maximum (Seyfferth et al., 2020). This near-channel location was previously found to contain no detectable sulfide and up to 1 mM ferrous iron in porewater in contrast to locations lower in elevation that were more strongly reducing and had up to 3 mM sulfide in solution and no detectable ferrous iron (Seyfferth et al., 2020).

Because we sought to capture changes in biogeochemistry as tides changed, we performed intensive sampling campaigns hourly over 24-hr. In an attempt to capture some seasonal variability, these 24-hr sampling campaigns were conducted once in the summer of 2020 during plant maturity and again in the spring of 2021 during plant green-up (Hill et al., 2021), hereafter referred to as summer and spring sampling events. The summer sampling event occurred during a new moon spring tide, while the spring sampling event occurred during a full moon spring tide. Spring tides were targeted to capture a wide range in tidal and redox amplitude over each tidal cycle.

2.2. In Situ Measurements

2.2.1. Multi-Level In Situ Redox Sensor

To capture rapid changes in redox with tidal oscillation, a platinum electrode redox sensor (Paleo Terra, Amsterdam, Netherlands) was inserted vertically into the soil 1 m from the tidal channel following previous methods

Version of Record at: https://doi.org/10.1029/2023JG007404

(Guimond, Seyfferth, et al., 2020). The sensor was connected to a data logger (Campbell Scientific, CR1000), which recorded a data point every 15 min. A reference potential was established by connecting a Calomel reference electrode (Fisher Scientific) to the data logger. The reference electrode was encased in a KCl salt bridge solution to establish a connection to the surrounding soil. The redox system was calibrated in the lab with known standards before deployment. A correction factor of +245 mV was added to the raw data to account for the difference in redox potential between the reference probe and the standard hydrogen electrode.

2.2.2. Hydrological Measurements

A groundwater well was previously installed approximately 1 m from the tidal channel (Seyfferth et al., 2020). A pressure transducer (Aqua TROLL 200 Data Logger) was inserted into the well, which collected a measurement every 15 min. In addition, an atmospheric pressure transducer (Baro-Driver) was installed aboveground near the well and was used to correct for atmospheric pressure to calculate water level elevation using software specifically designed for our transducers (Levelogger Version 4.5). Groundwater head is reported as elevation above (positive) or below (negative) ground surface.

Continuous surface water data was also collected in the tidal channel. The St. Jones Reserve manages a tidal channel sonde that records water level, salinity, water temperature, conductivity, pH, turbidity, and dissolved oxygen every 15 min. The surface water elevation data is reported as depth above (positive) or below (negative) the ground surface. Surface and groundwater level data were also used to calculate the hydraulic gradient between the channel bank groundwater and tidal channel surface water as the difference in head divided by the distance from the well to the channel bank, ∼1 m. Water level elevations were referenced to NAVD83.

2.3. Surface Water and Porewater Water Collection

Surface water from the tidal channel and soil porewater from the adjacent tidal channel bank were collected each hour simultaneously for 24 hr to connect porewater and surface water processes directly. Surface water was collected by rinsing an acid-washed 15 mL falcon tube with tidal channel surface water three times before collection. Porewater was collected from four rhizon samplers (Rhizosphere Research Products) fitted with ceramic filters (1.2 μm pore size). Rhizons were inserted into the soil at various depths 72 hr before sampling to allow equilibration before sample collection. Three rhizons were inserted horizontally into the channel bank at −6, −18, and −30 cm depth relative to the channel bank surface (hereafter referred to as R-6, R-18, and R-30. In addition, one rhizon was inserted vertically downward into the soil surface approximately 1m from the channel bank toward the marsh interior and near the groundwater well (hereafter referred to as R-Int) (Figure S2 in Supporting Information S1). Following previous methods, vacuum syringes were used to extract porewater from soil rhizons (Limmer et al., 2018).

The water samples (i.e., surface water and porewater) were split and used for various chemical analyses, taking care to minimize oxidation of porewater samples. One portion of the sample was immediately filtered in the field using 0.45 μm PTFE syringe filters, and aliquots were immediately placed into vials containing reagents used for colorimetric analysis of S^{2-} and Fe^{2+} using the Cline and Stookey methods, respectively (Cline, 1969; Stookey, 1970). We have successfully used this approach to measure sulfide and ferrous iron at the site (Northrup et al., 2018; Seyfferth et al., 2020). The remaining 0.45 μm-filtered sample was analyzed in the field with a calibrated electrode probe for pH (Orion Ross Ultra pH/ATC Triode). Another portion of the collected sample was used for carbon and nitrogen analyses after filtering 3 mL through Whatman GF/F filters (0.7 μm) in the laboratory. Most of the sample was analyzed for DOC, DIC, and total N (Vario TOC Cube, Elementar) while a subsample was used for Excitation Emission Matrices (EEMs) and Ultraviolet-Visible (UV-VIS) analysis on a fluorescence spectrophotometer (Aqualog, Horiba) to observe DOC source and composition. The Aqualog was calibrated using Double Deionized (DDI) blanks and data were normalized to the instrument's Raman Area. Wavelengths measured were between 230 and 700 nm with a measurement step of 2 nm. Fluorescence peak intensities (Coble A, C) and indices (HIX, BIX) were determined, as well as absorbance indices (Abs_{254}, S_r, $SUVA_{254}$, E_2: E_3). Previously established methods were followed for calculating these peaks and indices (Table S1 in Supporting Information S1).

2.4. Soil Gas Flux Measurements From the Channel Bank

Trace gas measurements (i.e., CO_2, CH_4 DMS) were collected from the soils/sediments of the channel bank to determine how the rising and falling tide affects gas exchange through the exposed pores of the channel bank.

Version of Record at: https://doi.org/10.1029/2023JG007404

Two PVC collars (20 cm diameter) were inserted horizontally into the side of the channel bank so that the center point aligned with 10 and 30 cm depth (Figure S2 in Supporting Information S1). These collars were inserted approximately 72 hr before the start of the sampling campaign to allow for soil equilibration before gas flux measurements. We clarify that these measurements do not represent water-atmosphere fluxes from the creek or surface fluxes of soil/sediment-atmosphere; rather, they represent soil/sediment-atmosphere fluxes from the channel bank. These soils/sediments are submerged during high tides and exposed during low tides, so while we targeted hourly flux measurements, we could not sample the collars when the water level was higher than the horizontally placed collars. Flux measurements were taken every hour (when possible) by fitting the soil collars with a PVC closed-loop chamber connected to a gas analyzer (DX4040, Gasmet Technologies, Finland) via gas-impermeable tubing. A small fan was attached to the inside of the chamber to allow the air to mix during measurements (Pearson et al., 2016). Measurements were taken every 5 s for approximately 3 min. Fluxes were calculated using the following equation:

$$\text{Soil Gas Flux} = \frac{\Delta c}{\Delta t}\frac{V}{S}\frac{\text{Pa}}{\text{RT}}$$

where c is the mole fraction of CO_2, CH_4, or DMS in μmol mol^{-1}, t is the observation time of 180 s, V is the total volume of the closed system, S is the surface area of the soil chamber, Pa is the atmospheric pressure, R is the universal gas constant, T is the surface soil temperature. We also measured N_2O, but these fluxes were very low and potentially under the instrument's detection limit, thus were not reported in this study. We followed standardized protocols, and a linear fit was applied to calculate $\Delta c/\Delta t$ (Limmer et al., 2018). We kept measurements for all gases if the changes in CO_2 concentrations had an R^2 value of ≥0.90, assuming that the collars' micrometeorological conditions were stable enough to calculate all gas fluxes following established protocols (Capooci & Vargas, 2022b; Petrakis et al., 2017). Because we could not make measurements when the collars were submerged during the highest tides, our data represent 16 summer and 15 spring measurements. All 16 measurements passed the data quality threshold during the summer, but 7 of the 15 measurements obtained during the spring were below our threshold and, therefore, are not included.

2.5. Statistical Analysis

Relationships between any two variables were assessed using bivariate linear regression ($\alpha = 0.05$). In addition, repeated measures analysis of variance (ANOVA) was performed to determine differences in tidal channel surface water and porewater biogeochemistry between data grouped in a variety of ways, including by hydraulic gradient direction (i.e., toward the channel or toward the channel bank soil) and groundwater direction (i.e., rising or falling). Significant differences between data groups were defined as having a p-value <0.05 and are represented with a p-value when only two groups are being assessed. When more than two data groups were evaluated, a repeated measures ANOVA was performed with a post hoc Tukey HSD test with significant differences between groups shown as different letters. All statistical analyses were performed using JMP Pro 16 (Version 16.2).

3. Results

3.1. Surface Water and Groundwater Hydrology

Two high tides and two low tides were studied across the two 24-hr monitoring periods (Figure 1). The water elevations are reported as depth above (+) or below (−) the near channel soil surface in the summer (Figure 1a) and spring (Figure 1b). Even though both summer and spring sampling events occurred during spring tides, the average height of the groundwater and surface water were significantly ($p < 0.0001$) different between events. The summer mean groundwater level was higher (20.1 ± 16.9 cm) than the spring (−7.3 ± 11.9 cm). The tidal channel mean level was also higher in the summer (37.4 ± 44.8 cm) than in the spring (13.3 ± 48.4 cm). The tidal channel amplitude in the summer was 137 cm (−87 to 50 cm), while in the spring, it was 126 cm (−86 to 40 cm). The groundwater amplitude in the summer was 53 cm (−2 to 51 cm), while in the spring, it was 36 cm (−23 to 13 cm). Notably, the groundwater level dropped minimally below the marsh surface (−2 cm) and only for a short period in the summer, while the drop in groundwater level in the spring was more substantial (−23 cm) and for hours at a time (Figure 1). While there were significant differences in surface water and groundwater amplitudes and ranges between summer and spring sampling campaigns, there were also differences in the hydraulic gradient between sampling events.

Version of Record at: https://doi.org/10.1029/2023JG007404

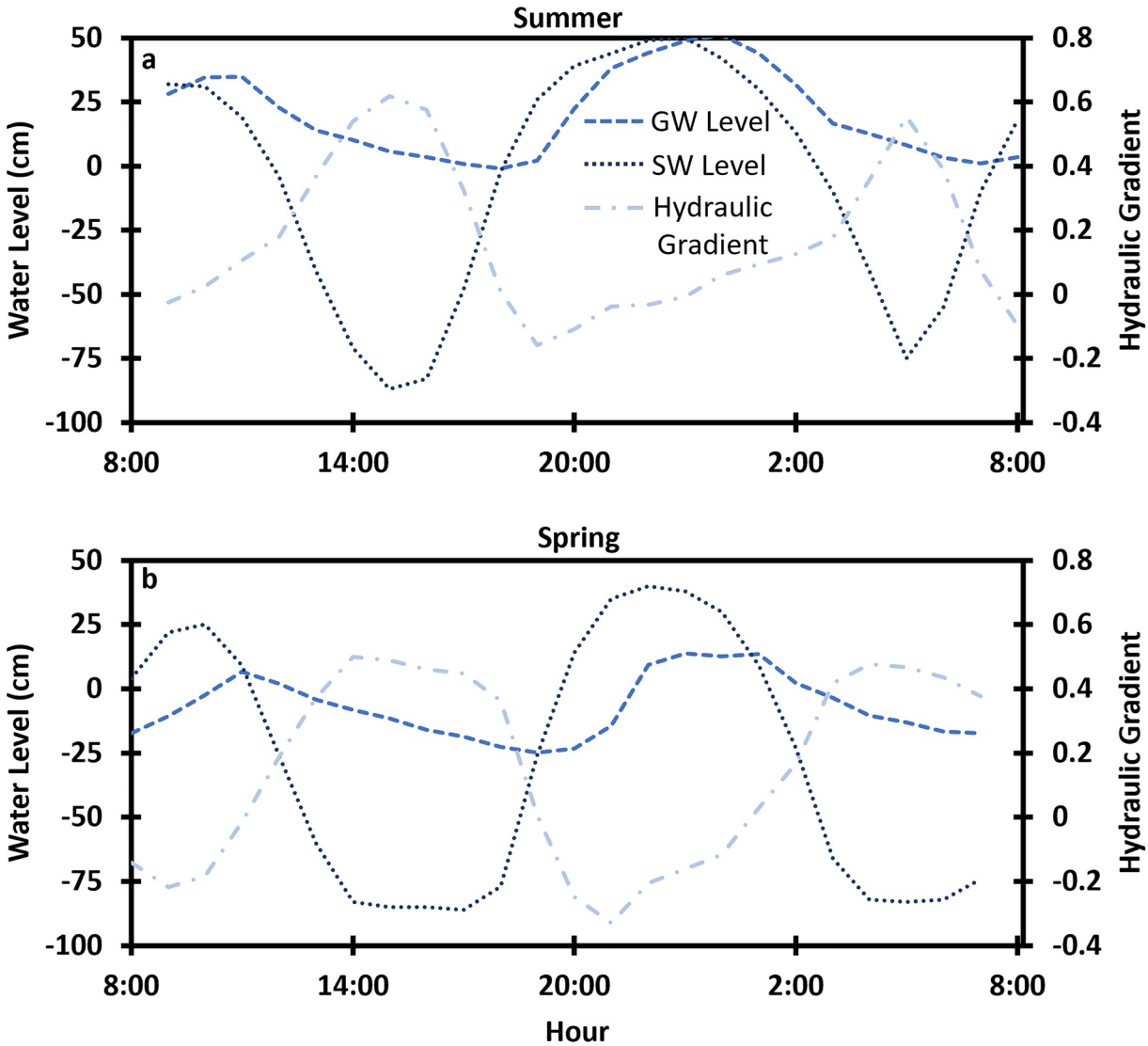

Figure 1. Groundwater (GW) in the channel bank, surface water (SW) in the tidal channel, and the hydraulic gradient between GW and SW across the 24-hr monitoring periods in the summer (a) and the spring (b). Water levels (GW and SW) are reported as depth above (+) or below (−) the near-channel soil surface.

Hydraulic gradients were derived from the groundwater and surface water elevations and varied over the 24-hr sampling events (Figure 2). The hydraulic gradient changed rapidly with tidal oscillation from negative gradients toward the channel bank soil to positive gradients toward the tidal channel, but the range and means for positive and negative gradients between summer and spring were similar. The mean hydraulic gradient in the summer (0.17 ± 0.30) was not significantly different ($p = 0.51$) from the mean hydraulic gradient in the spring (0.15 ± 0.25). Both spring and summer means were positive, which indicates that, on average, the hydraulic gradient was driving flow toward the tidal channel during both summer and spring sampling events. In the spring, the mean hydraulic gradient was significantly ($p < 0.0001$) higher during ebb tide (0.27 ± 0.24) than during flood tide (-0.01 ± 0.29). The summer hydraulic gradients were also significantly ($p = 0.002$) different between ebb (0.23 ± 0.21) and flood tides (0.09 ± 0.24). Differences in surface water and groundwater hydrology between and within summer and spring sampling events affected porewater biogeochemistry.

3.2. Porewater Biogeochemistry

Hydrologic tidal oscillation during the two sampling events altered porewater biogeochemistry. In situ redox potentials at multiple depths from the continuous datalogger were lowest when the groundwater levels were

Version of Record at: https://doi.org/10.1029/2023JG007404

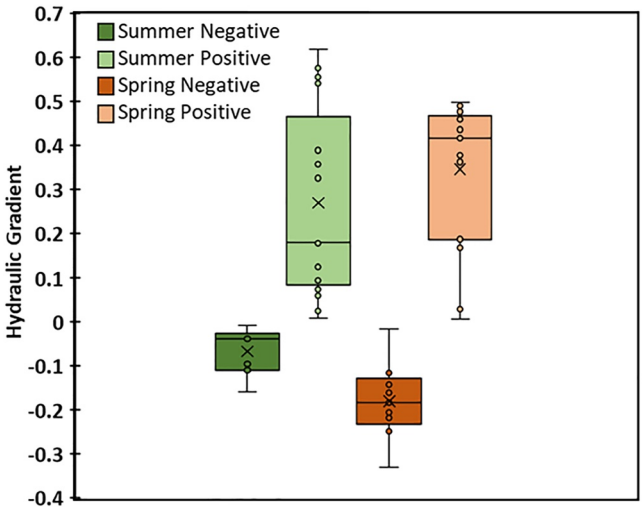

Figure 2. Box and whisker plot representing the variation in hydraulic gradients during the summer and spring sampling events, separated by positive and negative hydraulic gradients. Positive gradients indicate flow driven toward the tidal channel, while negative gradients indicate flow driven toward channel bank soils.

highest, forming negative linear trends with groundwater level, but differences existed between spring and summer sampling events (Figure 3). The mean summer redox potential averaged across all measured depths (−188.9 ± 0.8 mV) was significantly lower ($p < 0.0001$) than the spring redox potential (58.3 ± 174.5 mV). In addition, the range of porewater redox potentials in the summer (−190 to −187 mV) was much lower than the range in the spring (−117 to 373 mV). Although the soil redox potential was significantly correlated to groundwater level in both seasons, the relationships were weaker in the summer than in the spring. In the summer, the groundwater level only dropped to 2 cm below the ground surface, resulting in strongly reducing conditions throughout the entire 24-hr monitoring period. In the spring, the groundwater level dropped well below the surface (−23 cm), causing spikes in soil redox potential during each low tide down to the 23 cm depth of the redox probe, but was consistently reducing at the 43 cm depth, consistent with the groundwater table elevation. These hydrologically driven redox oscillations affected redox-sensitive solutes.

Porewater data from the vertical profile of channel bank rhizons (R-6, R-18, R-30) were assessed based on whether the groundwater level rose or fell during sampling (Table 1). In the spring, reduced Fe (Fe^{2+}) had a significantly higher mean when the groundwater level was rising (0.04 ± 0.03 mM) compared to when the groundwater level was falling (0.02 ± 0.02 mM). Summer Fe^{2+} concentrations did not change significantly between falling (0.03 ± 0.02 mM) and rising (0.04 ± 0.02 mM) groundwater levels, consistent with minimal redox oscillation in the summer. In the spring, DOC was significantly higher during rising groundwater (1.65 ± 1.72 mM) compared to falling groundwater (0.95 ± 0.29 mM), while in the summer, there was no significant difference in DOC concentrations between falling and rising groundwater. DOC and Fe^{2+} concentrations varied across the 24-hr sampling campaigns (Figure S3 in Supporting Information S1) and formed a positive and significant relationship during both flood and ebb tide in the summer while only forming a significant relationship in the spring during flood tide (Figure 4). While porewater Fe^{2+} and DOC were affected by the tidal oscillation and thus redox state of the soils, porewater biogeochemistry also changed with depth.

Porewater variables changed with depth and proximity from the channel and differed between spring and summer sampling campaigns (Figure 5). In the summer, porewater pH and DIC increased with depth, Fe^{2+} slightly decreased with depth, and neither DOC nor TN changed with depth. Abs_{254}, a proxy for aromatic DOC, increased with depth and E_2:E_3, inverse to molecular weight, was highest at the surface and decreased with depth. This indicates that DOC aromaticity and molecular weight generally increased with depth. Terrestrial C signals derived from EEMs indices (Coble A and C) also increased with depth, while the Biological Index (BIX) did not change with depth.

At R-Int, which sampled vertically down from 0 to 10 cm depth approximately 1 m from the channel bank in a more densely planted area, porewater chemistry differed from the channel bank porewater in summer. The R-Int pH, DIC, DOC, and TN were higher than those from the channel bank while Fe^{2+} was lower. The OC:TN ratio was approximately three times higher at R-Int than the channel bank rhizons. R-Int also had a stronger terrestrial signal (Coble A and C peak) and a higher Abs_{254}. These results indicate both changes with channel-bank depth and distance from the channel bank.

Porewater chemistry was different during the spring campaign. In the spring, concentrations of Fe^{2+} did not change with depth, nor did DOC. Unlike the summer, spring DIC concentrations decreased with depth, but R-Int still had the highest mean DIC value. There was no change in the DOC:TN ratio with depth in spring. Spring UV-VIS data had different patterns with depth and distance from the channel than in the summer. Abs_{254} did not change with depth and was lowest at R-Int. Coble A decreased with depth and was lowest at R-Int during spring, opposite from what was observed in the summer. This indicates that terrestrial C decreased with depth and with distance from the tidal channel in the spring. The BIX remained consistent with depth and distance from the channel in spring. In the spring, porewater concentrations of Fe^{2+} were significantly lower than in the summer (Table 2). DOC concentrations were significantly lower in the spring than in the summer. The pH was higher

Version of Record at: https://doi.org/10.1029/2023JG007404

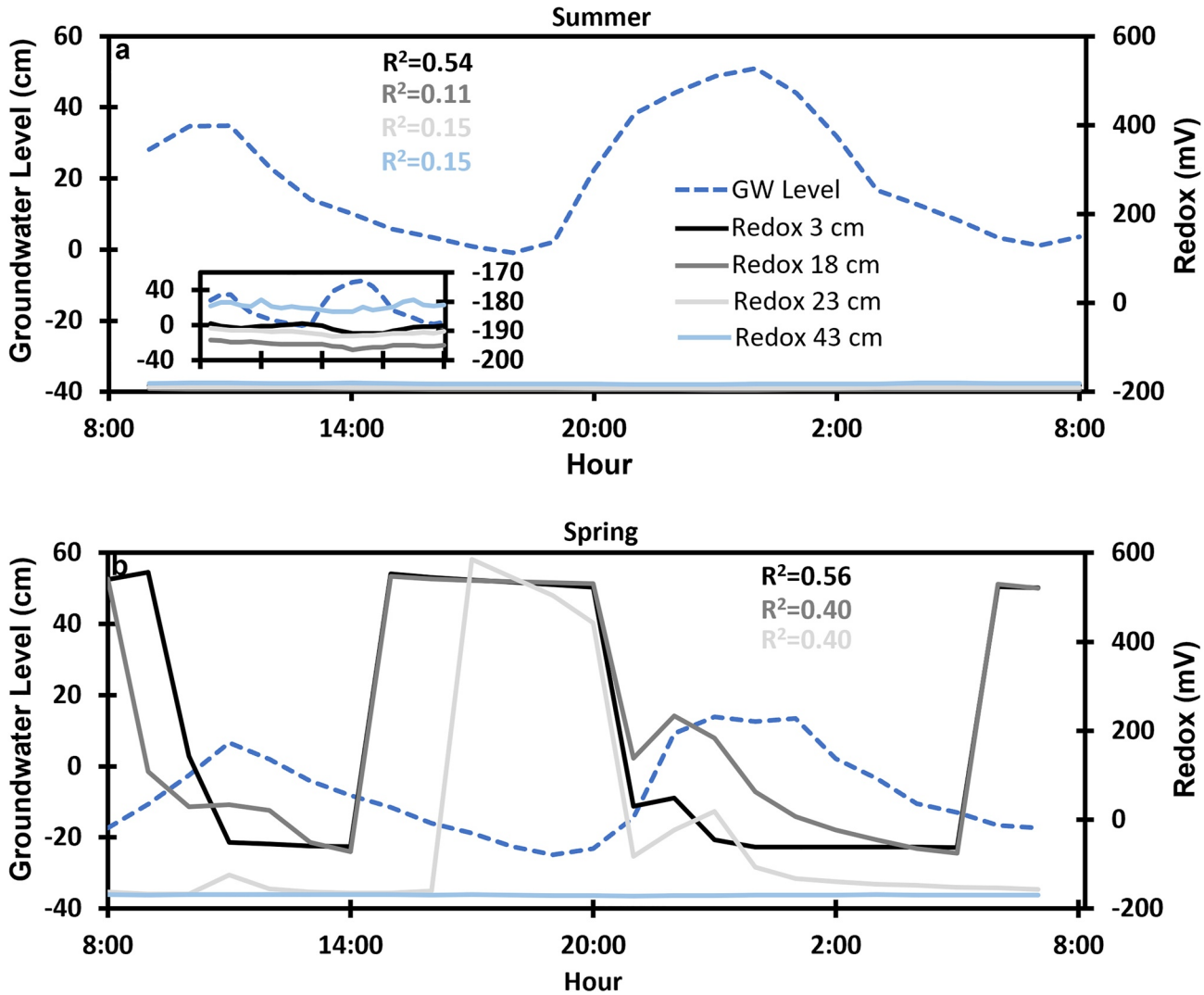

Figure 3. Redox conditions of soils were different between sampling events due to hydrology. In situ redox at 3, 18, 23 and 43 cm below ground surface plotted with groundwater level for summer (a) and spring (b). R^2 values are reported from bivariate linear regression between groundwater and respective redox depth. Only significant ($p < 0.05$) trends are reported. The inset in (a) has a *y*-axis range of only 20 mV to illustrate how little redox potential varied during the summer sampling event.

in the summer, while the salinity was lower. The spring Abs_{254} mean was approximately three times lower than in the summer, while the E_2:E_3 ratio was about twice as high in the spring. This indicates that spring DOC was less aromatic with a lower molecular weight than summer DOC. Coble A and C peaks were approximately three times lower in the spring. The BIX was significantly higher in the spring than in the summer, indicating that spring DOC had a higher microbial source. The S_r was also higher in the spring, indicative of increased microbial marine-derived C. The HIX was significantly higher in the summer, indicating increased humification during summer compared to spring.

3.3. Surface Water Biogeochemistry

Seasonal differences in the biogeochemistry of the tidal channel surface water were apparent, as most measured variables significantly differed across summer and spring sampling events (Table 3). Tidal channel DOC levels and the terrestrial signal (Coble A & C) were about twice as high in the summer than in the spring. Abs_{254} was significantly higher in the summer, indicating that summer surface water DOC was more aromatic than in the spring. TN levels were significantly higher in the spring than in the summer by an order of magnitude. The BIX was higher in the spring, indicating that spring surface water DOC had an increased marine-like signature.

Version of Record at: https://doi.org/10.1029/2023JG007404

Table 1
Results of Repeated Measures ANOVA From Averaged Porewater Data Between Periods When the Groundwater Was Either Rising or Falling in the Summer and Spring

	Summer			Spring		
Variable	Falling groundwater	Rising groundwater	*P*-value	Falling groundwater	Rising groundwater	*P*-value
Fe^{2+} (mM)	0.03 (0.02)	0.04 (0.02)	0.33	0.02 (0.02)	0.04 (0.03)	**0.001**
Sulfide (mM)	0.003 (0.003)	0.003 (0.003)	0.27	No Data	No Data	No Data
pH	8.10 (0.50)	8.24 (0.67)	0.36	7.50 (0.37)	7.45 (0.18)	0.77
Salinity (ppt)	7.39 (0.67)	7.24 (0.90)	0.64	8.64 (1.06)	9.26 (1.63)	0.11
Sr	0.93 (0.18)	0.94 (0.17)	0.66	1.07 (0.43)	0.96 (0.38)	0.38
ABS_{254}	0.78 (0.19)	0.89 (0.43)	0.15	0.23 (0.07)	0.22 (0.08)	0.82
Coble A	6.84 (1.32)	6.85 (1.81)	0.98	2.29 (0.50)	2.40 (0.58)	0.43
Coble C	3.59 (0.67)	3.66 (1.11)	0.73	1.19 (0.28)	1.23 (0.33)	0.63
HIX	8.51 (2.45)	8.01 (3.12)	0.45	3.90 (1.25)	3.41 (1.50)	0.15
BIX	0.58 (0.02)	0.57 (0.02)	0.29	0.69 (0.02)	0.69 (0.04)	0.60
DOC (mM)	1.89 (0.51)	1.99 (0.68)	0.47	0.95 (0.29)	1.65 (1.72)	**0.01**
DIC (mM)	4.67 (1.35)	4.43 (1.44)	0.47	2.24 (0.64)	2.28 (0.69)	0.82
TC (mM)	6.57 (1.50)	6.42 (1.62)	0.71	3.20 (0.67)	3.90 (1.50)	**0.01**
TN (mM)	0.10 (0.02)	0.11 (0.03)	**0.02**	0.08 (0.07)	0.14 (0.11)	**0.004**
OC:N	19.80 (4.85)	18.42 (4.80)	0.25	19.82 (17.10)	16.41 (14.77)	0.42
SUVA254	0.34 (0.20)	0.37 (0.16)	0.46	0.25 (0.07)	0.20 (0.10)	**0.03**
E2:E3	5.59 (0.89)	5.84 (1.20)	0.30	10.75 (16.90)	12.75 (12.30)	0.63

Note. Values are the means (±SD) of the vertical profile of channel bank rhizons (R-6, R-18, R-30). Significant differences ($p < 0.05$) are indicated in bold.

Continuous water quality data (salinity, pH, redox, temperature, dissolved oxygen, turbidity) measured from the tidal channel sonde probe was also collected (Figure S4 in Supporting Information S1). All continuously measured variables were significantly different ($p < 0.05$) between seasons. Salinity (12.4 ± 4.7 ppt) was higher in spring than in summer (7.5 ± 3.9 ppt) and, for both seasons, tended to increase with the rising tide. The pH was higher in the spring (7.2 ± 0.4) than in the summer (7.0 ± 0.3), while redox potential was lower in the spring (−30.5 ± 21.8 mV) than in the summer (−2.1 ± 15.5 mV), though both seasons on average had reducing surface water. Spring surface water temperatures (23.6 ± 2.5°C) were cooler than in the summer (25.2 ± 1.2°C), leading to higher dissolved oxygen levels in the spring (5.7 ± 5.3 mg L^{-1}) than in the summer (2.7 ± 1.9 mg L^{-1}). Turbidity values were almost twice as high in the spring (73.7 ± 32.11 NTU) than in the summer (41.0 ± 21.4 NTU).

Surface water data was further assessed based on the hydraulic gradient between surface and groundwater. Positive gradients drive flow toward the channel, while negative gradients drive the flow into the channel bank. Tidal channel Fe^{2+} concentration increased significantly with the hydraulic gradient during spring and summer (Figure 6). DOC and the Coble peaks (A & C) also increased significantly with hydraulic gradient, but only in the spring. In contrast, BIX ($R^2 = 0.31$), S_r ($R^2 = 0.19$), and salinity ($R^2 = 0.29$) formed significant negative relationships with the hydraulic gradient in the spring only. In the summer, BIX, S_r, and salinity did not include significant relationships with hydraulic gradient.

Significant differences in means of many of the measured biogeochemical variables between times of positive and negative hydraulic gradients were observed in the spring (Table 4b). During the spring sampling event, there were significantly higher Fe^{2+}, DOC, DIC, Coble A & C peaks, HIX, and Abs254 in the channel when the hydraulic gradient was driving flow toward the channel than when the flow was into the channel bank. In contrast, when the gradient drove flow toward the bank, surface water BIX, S_r, and salinity were significantly higher. This was not the case during the summer sampling event, as there were no significant differences in biogeochemistry between hydraulic gradient directions (Table 4a), except for total nitrogen (TN). These results indicate differences

Version of Record at: https://doi.org/10.1029/2023JG007404

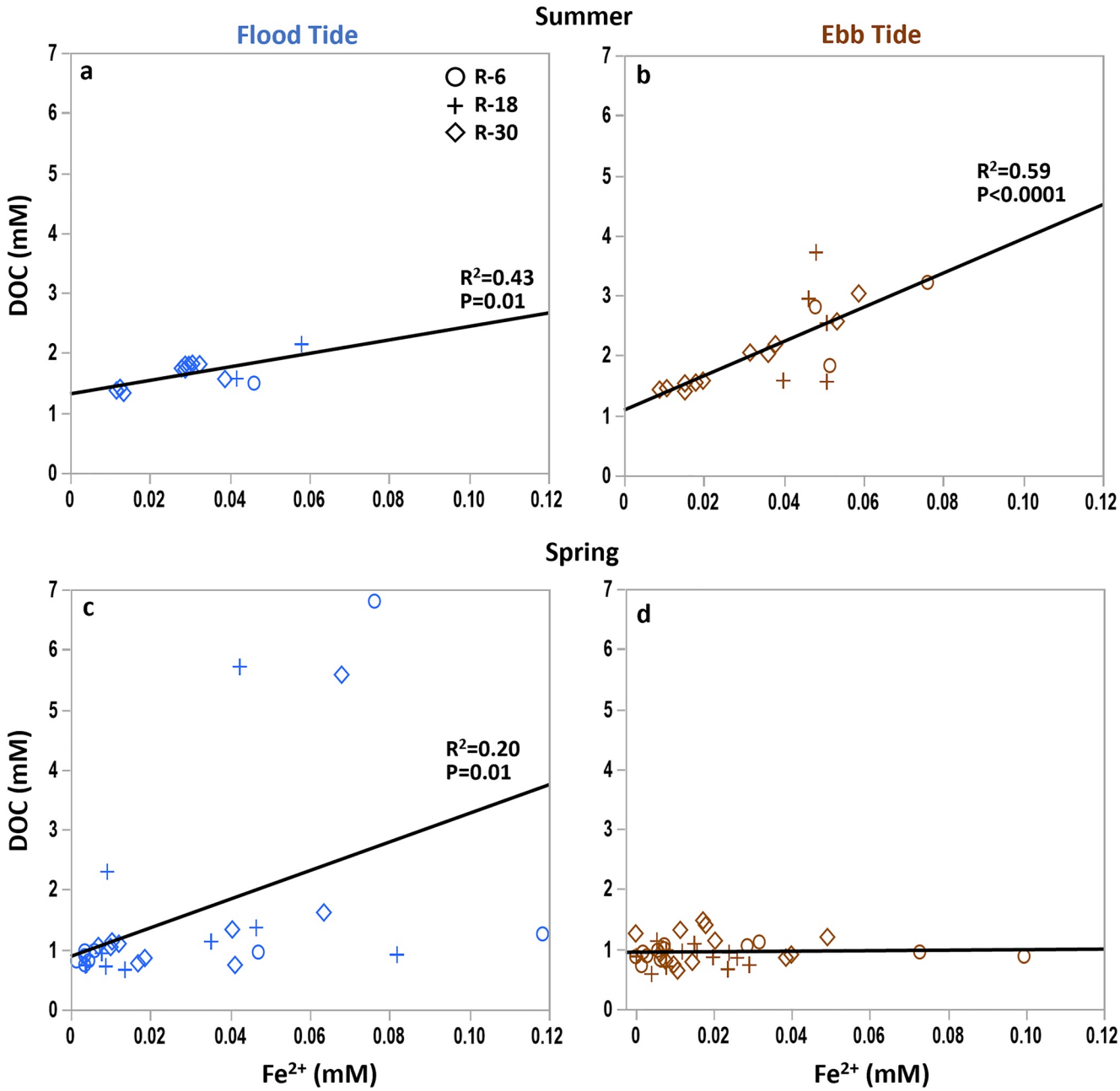

Figure 4. Relationships between DOC and Fe^{2+} for the summer (a–b) and the spring (c–d) from porewater samples at the three different rhizons installed at the channel bank (R-6, R-18, R-30). The data has been split up based on periods of ebb and flood tides. R^2 values result from a bivariate linear regression where $p < 0.05$ for a–c, but not d.

in the source and concentration of solutes in the channel based on the flow direction between the marsh platform groundwater and tidal channel surface water, but these patterns changed between summer and spring sampling events.

3.4. Soil Trace Gas Fluxes From the Channel Bank

Soil trace gases from the channel bank were measured to assess horizontal gas movement seasonally and with hydrologic oscillation (Figure 7). In the summer, CO_2 flux from the 10 cm collar was significantly ($p < 0.0001$) higher (0.08 ± 0.06 μmol m^{-2} s^{-1}) than in the spring (0.02 ± 0.02 μmol m^{-2} s^{-1}) but this trend was opposite for the 30 cm collar where CO_2 flux was higher in the spring (0.12 ± 0.16 μmol m^{-2} s^{-1}) than in the

Version of Record at: https://doi.org/10.1029/2023JG007404

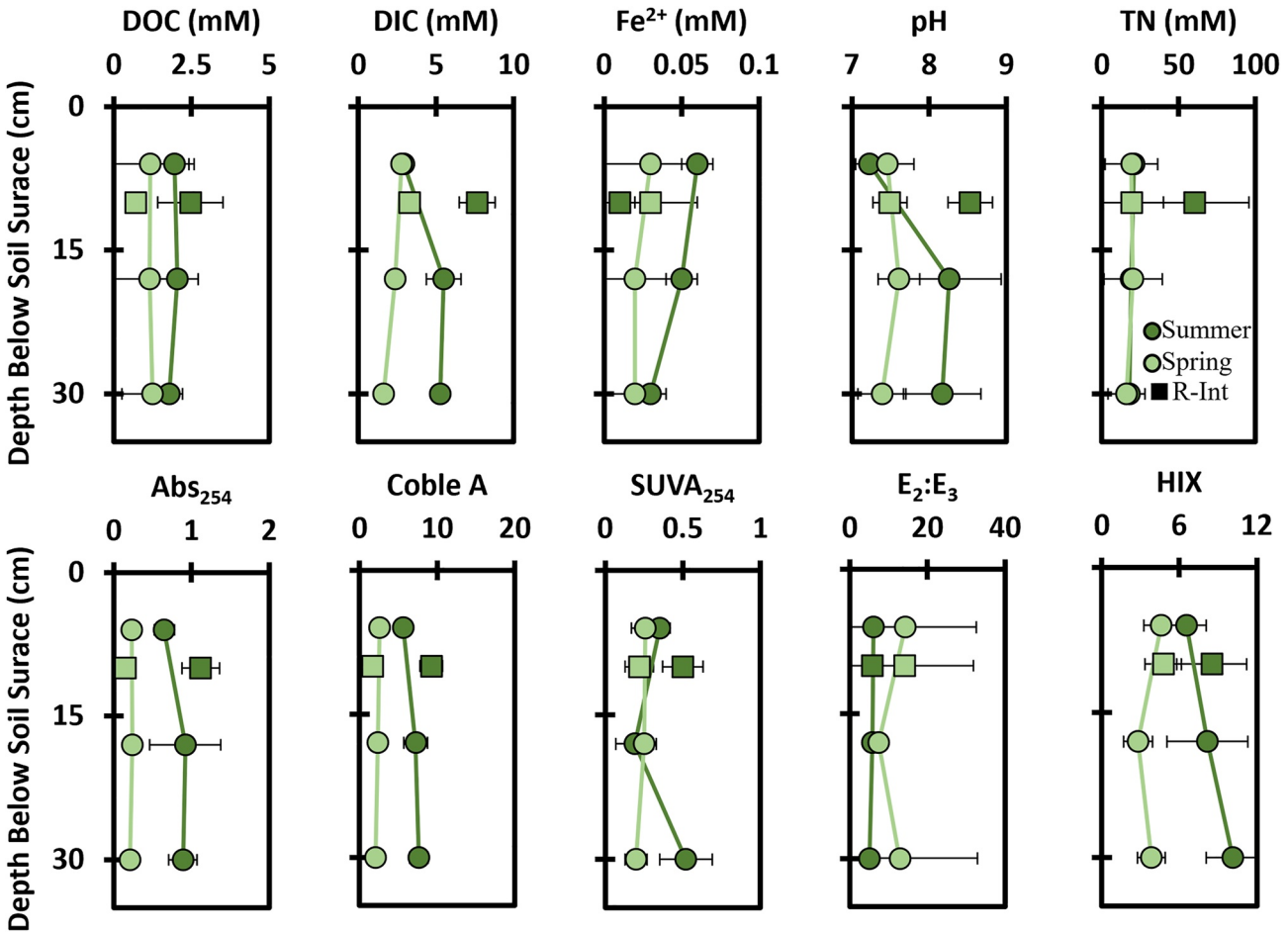

Figure 5. Depth profiles for rhizons placed horizontally in the channel bank at −6 cm (R-6), −18 cm (R-18), and −30 cm (R-30) relative to the channel bank soil surface. The interior rhizon (R-Int) placed vertically into the soil approximately 1 m from the channel bank is plotted as its own point at 10 cm. The points represent the average across the 24-hr sampling (±SD).

summer (0.08 ± 0.03 μmol m^{-2} s^{-1}), but these means were not significantly different (p = 0.12). The CH_4 flux from the 10 cm collar was significantly ($p < 0.0001$) higher in the summer (0.47 ± 0.61 nmol m^{-2} s^{-1}) than in the spring (0.02 ± 0.04 nmol m^{-2} s^{-1}), while the 30 cm collar was not significantly (p = 0.36) different between spring (1.18 ± 2.73 nmol m^{-2} s^{-1}) and summer (1.63 ± 1.38 nmol m^{-2} s^{-1}). DMS from the 10 cm collar was significantly ($p < 0.0001$) higher in the summer (0.38 ± 0.26 nmol m^{-2} s^{-1}) than in the spring (0.10 ± 0.09 nmol m^{-2} s^{-1}), while the 30 cm collar was also significantly ($p < 0.0001$) higher in the summer (0.45 ± 0.24 nmol m^{-2} s^{-1}) than in the spring (0.14 ± 0.11 nmol m^{-2} s^{-1}). Variability in the gas flux data is not only apparent between sampling events but also between the depths, particularly for CH_4. When spring and summer data sets are combined, the 30 cm collar (1.903 ± 2.71 nmol m^{-2} s^{-1}) emitted significantly more CH_4 than the 10 cm collar (0.27 ± 0.52 nmol m^{-2} s^{-1}), while there was no significant difference between depths for CO_2 and DMS. Trace gas fluxes changed not only with seasonality and depth but also with groundwater level oscillation.

We observed several significant relationships between the groundwater level and trace gas fluxes. In the spring, DMS flux at the 10 cm collar increased significantly (R^2 = 0.52, $p < 0.0001$) with the groundwater table elevation. A similar positive relationship with groundwater level exists with CO_2 at the 30 cm collar in the summer (R^2 = 0.51, $p < 0.0001$). When spring and summer data sets are combined, DMS is significantly and positively correlated with groundwater level at both the 10 cm collar (R^2 = 0.27) and the 30 cm collar (R^2 = 0.51). CH_4 did not form any significant relationship with groundwater level. These positive relationships between groundwater level and DMS and CO_2 flux suggest a mechanism in which these gases are likely pushed upward and outward from the channel bank with the tides.

Version of Record at: https://doi.org/10.1029/2023JG007404

Table 2
Results of Repeated Measures ANOVA of Porewater Data Between Spring and Summer Sampling Events

Variable	Spring	Summer	*P*-value
Fe^{2+} (mM)	0.02 (0.03)	0.03 (0.02)	**0.02**
pH	7.47 (0.31)	8.14 (0.58)	**<0.0001**
Salinity (ppt)	8.54 (1.49)	7.33 (0.76)	**0.0004**
Sr	1.04 (0.42)	0.93 (0.18)	0.06
ABS_{254}	0.22 (0.07)	0.82 (0.31)	**<0.0001**
Coble A	2.33 (0.53)	6.84 (1.52)	**<0.0001**
Coble C	1.12 (0.29)	3.62 (0.90)	**<0.0001**
HIX	3.73 (1.37)	8.31 (2.73)	**<0.0001**
BIX	0.69 (0.03)	0.58 (0.02)	**<0.0001**
DOC (mM)	1.19 (1.08)	1.93 (0.58)	**<0.0001**
DIC (mM)	3.45 (1.09)	6.51 (1.54)	**<0.0001**
TC (mM)	3.59 (0.99)	7.31 (2.14)	**<0.0001**
TN (mM)	0.10 (0.09)	0.10 (0.02)	0.88
OC:N	18.52 (16.22)	19.25 (4.83)	0.72
SUVA254	0.24 (0.08)	0.35 (0.19)	**<0.0001**
E2:E3	11.40 (15.51)	5.69 (1.03)	**0.003**

Note. Numbers are the means (±SD) among the channel bank rhizons (R-6, R-18, R-30) across the 24 hr sampling events. Significant differences ($p < 0.05$) are indicated in bold.

Table 3
Results of Repeated Measures ANOVA From Tidal Channel Surface Water Data Between Summer and Spring Sampling Events

Variable	Spring	Summer	*P*-value
Fe^{2+} (mM)	0.01 (0.01)	0.01 (0.01)	0.21
Sulfide (mM)	0.01 (0.003)	0.002 (0.001)	**<0.0001**
pH	7.10 (0.10)	6.65 (0.10)	**0.002**
Salinity (ppt)	9.15 (3.22)	7.00 (3.38)	**0.03**
Sr	1.14 (0.71)	0.86 (0.11)	0.07
ABS_{254}	0.22 (0.07)	0.38 (0.12)	**<0.0001**
Coble A	1.72 (0.75)	2.96 (1.04)	**<0.0001**
Coble C	0.88 (0.42)	1.57 (0.47)	**<0.0001**
HIX	4.27 (1.89)	6.36 (1.79)	**0.0003**
BIX	0.70 (0.06)	0.62 (0.04)	**<0.0001**
DOC (mM)	0.66 (0.17)	0.96 (0.23)	**<0.0001**
DIC (mM)	1.35 (0.43)	1.28 (0.67)	0.64
TC (mM)	2.02 (0.57)	2.24 (0.73)	0.25
TN (mM)	0.17 (0.13)	0.04 (0.02)	**<0.0001**
OC:N	9.27 (16.01)	29.41 (18.49)	**0.0002**
SUVA254	0.34 (0.10)	0.39 (0.08)	**0.03**
E2:E3	5.0 (1.14)	5.36 (0.70)	0.20

Note. Numbers are the means across the 24 hr sampling events (±SD). Significant differences ($p < 0.05$) are indicated in bold.

4. Discussion

4.1. Variability of CDOM Across Seasons

The spring and summer sampling events had significantly different chromophoric dissolved organic carbon (CDOM) concentrations and properties in both the porewater and tidal channel surface water, indicating high seasonal variability of CDOM concentration, source, and processing. Coble A and C peaks correlate well with soil humics and terrestrially derived C (Baker et al., 2008; Cory et al., 2010). Indices such as S_r and the BIX correlate well with marine-derived microbial C, such as phytoplankton from the adjacent bay (Helms et al., 2008; Huguet et al., 2009). In the spring, the CDOM signature observed in both the porewater and surface water from the tidal channel indicates more algal contributions, as reflected by a higher BIX and S_r than in summer. This could be caused by benthic microalgae growing on the marsh platform surface because the soil surface would not be fully shaded from the cordgrass in the spring and may also be due to the import of marine C from the adjacent bay. By the summer, *Spartina* is well established and exudes C into the porewater, likely via root exudation. This is reflected in the much higher average porewater DOC concentration in the summer and the higher DOC concentration in the channel. Fresh inputs of C will stimulate soil microbial processing of CDOM, yielding an increased humic-like signature. The data reflects these observations because the summer CDOM signature is more terrestrial (Coble A and C peaks), humic (HIX), and aromatic ($SUVA_{254}$). Greater microbial processing and plant activity (i.e., root respiration) in the summer is also supported by significantly higher porewater DIC concentrations, as DIC is partially controlled by microbial degradation of DOC and respiration from microbes and plant roots. These data demonstrate changes in the seasonal characteristics of porewater C and CDOM with potential implications for tidal channel waters to which they may be laterally exported. We also found higher DOC and terrestrial like CDOM, especially in the summer at R-Int where plants were denser than our vertical transect along the channel bank (R-6, R-18, R30). Considering both the temporal and spatial variability of lateral and horizontal C fluxes is essential because the source, characteristics, and concentrations change among seasons and distance from the tidal channel. While these changes in CDOM seem to be related to primary productivity and seasonality, our sampling design represents only one 24 hr time point in each season. Therefore, we cannot rule out alternative explanations, such as changes in hydraulic gradients and tidal flooding regimes. We suggest future studies link porewater and surface water horizontal exchange over extended periods of time and across different sections of banks along creek channels.

4.2. Fe Oxides Affect DOC Mobility

We hypothesized that Fe oxides stabilize DOC in the solid phase during periods of soil oxidation (ebb tide), while these Fe-DOC associations dissolve during periods of soil reduction (flood tide). Our data support this hypothesis and provide insight into these tidally driven chemical processes affecting the horizontal transport of DOC. During flood tide in both the spring and summer events, porewater DOC and Fe^{2+} in channel bank soils formed significant and positive relationships. This can be interpreted as the destabilization of Fe-DOC solid-phase assemblages as Fe-reducing bacteria reductively dissolve C-bearing Fe oxides under reducing conditions during flood ties, causing Fe and DOC to enter the solution phase together (Fettrow et al., 2023; Hagedorn et al., 2000; Wordofa et al., 2019). The dissolution of Fe can also result from biological siderophores in which microbially produced

Version of Record at: https://doi.org/10.1029/2023JG007404

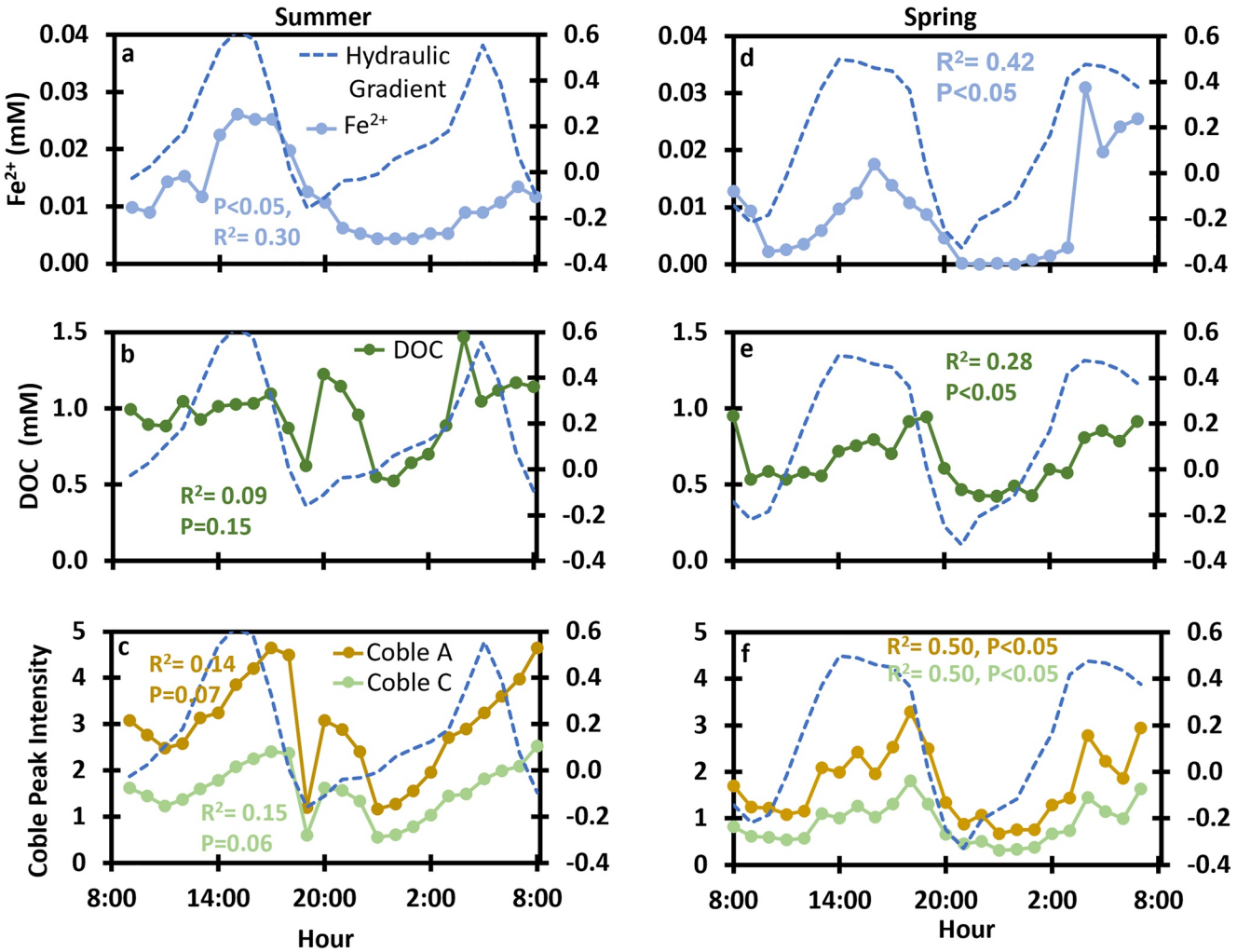

Figure 6. Plots of the hydraulic gradient with biogeochemical variables from tidal channel surface water samples. Plots (a–c) are from the summer, while panels (d–f) are from the spring. *P*-values and R^2 values result from bivariate linear regression between biogeochemical variables and the gradient.

organic acids directly dissolve Fe oxides (Parrello et al., 2016). The positive relationship between Fe^{2+} and DOC was expected during periods of flood tide when tidal inundation causes several hours of reducing soil conditions. The summer sampling event experienced flooded conditions and strongly reducing soil conditions throughout the entire 24-hr monitoring period due to the higher tide. Because the strongly reducing redox potential of the soils did not change between flood and ebb tide during the summer sampling event, the Fe and DOC likely remained in solution throughout the entire 24-hr monitoring period, as evidenced by the significant relationships between Fe^{2+} and DOC concentrations for both flood and ebb tide in the summer (Figure 4). Fe oxides are sensitive to flood duration and recent evidence suggests that continuous inundation from sea level rise will decrease Fe-C coprecipitate formation and increase the horizontal/lateral C flux (Fettrow et al., 2023).

As the tide receded and ebb tide persisted, oxygen flowed into the soil pore spaces, causing an increase in soil redox potential. This was evident in the spring during ebb tide and was the point at which the relationship between porewater Fe^{2+} and DOC did not form a significant positive relationship. Previously dissolved Fe^{2+} may have reacted with oxygen, causing Fe^{2+} and DOC to coprecipitate and thus lower the concentration in the solution phase. In laboratory incubations, we observed such relationships where ebb tides caused the formation of Fe-C coprecipitates that lowered DOC concentrations (Fettrow et al., 2023). Coprecipitation can occur in less than 30 min of oxygen exposure and readily occurs in environments that experience periodic flooding and drying (Riedel et al., 2013; Sodano et al., 2017). The conditions necessary for this reaction were exhibited during the spring sampling event when the groundwater level dropped well below the surface (−23 cm), allowing the soil

Version of Record at: https://doi.org/10.1029/2023JG007404

Table 4
Results of Repeated Measures ANOVA From Tidal Channel Surface Water Data Between Periods When the Hydraulic Gradient Was Either Toward the Channel (+) or the Channel Bank Soil in the Summer and Spring

	Summer			Spring		
Variable	Toward channel	Toward soil	*P*-value	Toward channel	Toward soil	*P*-value
Fe^{2+} (mM)	0.01 (0.01)	0.01 (0.00)	0.12	0.01 (0.01)	0.004 (0.00)	**0.01**
Sulfide (mM)	0.002 (0.00)	0.002 (0.00)	0.65	0.01 (0.00)	0.01 (0.00)	0.30
pH	6.62 (0.69)	6.72 (0.34)	0.71	7.17 (0.27)	6.99 (0.28)	0.14
Salinity (ppt)	7.28 (3.11)	6.31 (4.16)	0.53	7.93 (2.68)	11.18 (3.12)	**0.01**
Sr	0.88 (0.11)	0.83 (0.09)	0.33	0.92 (0.20)	1.50 (1.07)	**0.04**
ABS_{254}	0.38 (0.11)	0.36 (0.16)	0.70	0.25 (0.07)	0.17 (0.05)	**0.007**
Coble A	3.09 (0.97)	2.63 (1.21)	0.34	2.08 (0.70)	1.11 (0.32)	**0.001**
Coble C	1.64 (0.54)	1.40 (0.68)	0.38	1.09 (0.39)	0.54 (0.16)	**0.001**
HIX	6.60 (1.76)	5.76 (1.89)	0.31	4.91 (2.00)	3.19 (1.11)	**0.03**
BIX	0.62 (0.04)	0.62 (0.06)	0.93	0.67 (0.05)	0.75 (0.05)	**0.003**
DOC (mM)	0.96 (0.22)	0.95 (0.26)	0.90	0.73 (0.15)	0.56 (0.16)	**0.02**
DIC (mM)	1.41 (0.74)	0.95 (0.26)	0.13	1.51 (0.47)	1.09 (0.14)	**0.02**
TC (mM)	2.38 (0.81)	1.90 (0.35)	0.15	2.24 (0.59)	1.65 (0.29)	**0.01**
TN (mM)	0.04 (0.01)	0.05 (0.03)	**0.04**	0.16 (0.15)	0.18 (0.12)	0.73
OC:N	32.90 (20.23)	20.94 (10.00)	0.15	11.66 (19.83)	5.57 (6.34)	0.39
SUVA254	0.40 (0.08)	0.37 (0.09)	0.38	0.34 (0.06)	0.33 (0.15)	0.72
E2:E3	5.33 (0.68)	5.44 (0.81)	0.73	5.12 (0.78)	4.81 (1.61)	0.54

Note. Numbers are the means (±SD). Significant differences ($p < 0.05$) are indicated in bold.

redox to increase to ~550 mV. In contrast, these conditions were not detected during the summer sampling event when groundwater levels remained near or above the surface during the 24-hr monitoring period. These results highlight hydrologic control on Fe-oxide retention mechanisms of DOC in variably flooded environments, and the differences between seasons and tidal patterns likely contribute to the high uncertainty of lateral C movement from coastal environments (Hayes et al., 2018). Our evidence suggests that Fe oxide coprecipitation and dissolution between ebb and flood tides partially controls the horizontal flux of DOC to the tidal channel.

A variety of Fe-bearing minerals likely interacted with dissolved carbon in this study. While ferrihydrite makes up the largest fraction of Fe minerals in bulk soil at the tested field site (Seyfferth et al., 2020) and is likely the main Fe oxide contributing to coprecipitate formation (Sodano et al., 2017) because of its high reactivity, S-containing minerals including pyrite (FeS_2) and jarosite are also present (Fettrow et al., 2023; Seyfferth et al., 2020). Jarosite often is found in tidal wetlands due to pyrite oxidization (Keene et al., 2010), that is, during ebb tides. Jarosite has previously been shown to protect root residue from microbial turnover through inclusion (Pohl et al., 2021). Thus, jarosite and ferrihydrite likely played roles in carbon retention during ebb tides. In addition to bulk soil, forming Fe oxide-rich root plaque on and near wetland plant roots may have also contributed to C storage, as these are known reservoirs of C in coastal wetlands (C. Yu et al., 2021; Zhang et al., 2021). While we do not have evidence of root plaque in our study, R-Int tended to have less Fe^{2+} than rhizons along the channel bank, indicative of more soil aeration via root aerenchyma and precipitation of Fe in the rhizosphere, likely due to higher plant activity and root biomass at R-Int. Fe root plaque may further decrease the mobility of DOC during horizontal transport to the tidal channel. Future studies should closely consider the role Fe root plaque may play in the horizontal C flux, as well as the seasonal variability of Fe mineral-C dynamics.

4.3. Horizontal Exchange of Solutes Between the Marsh Platform and the Tidal Channel

Our data support the hypothesis that the hydraulic gradient controls the physical exchange of solutes between the channel bank groundwater and the surface water of the tidal channel, regulating the concentration and source of C horizontal fluxes to tidal channels. We observed significant relationships between the concentration and source

Version of Record at: https://doi.org/10.1029/2023JG007404

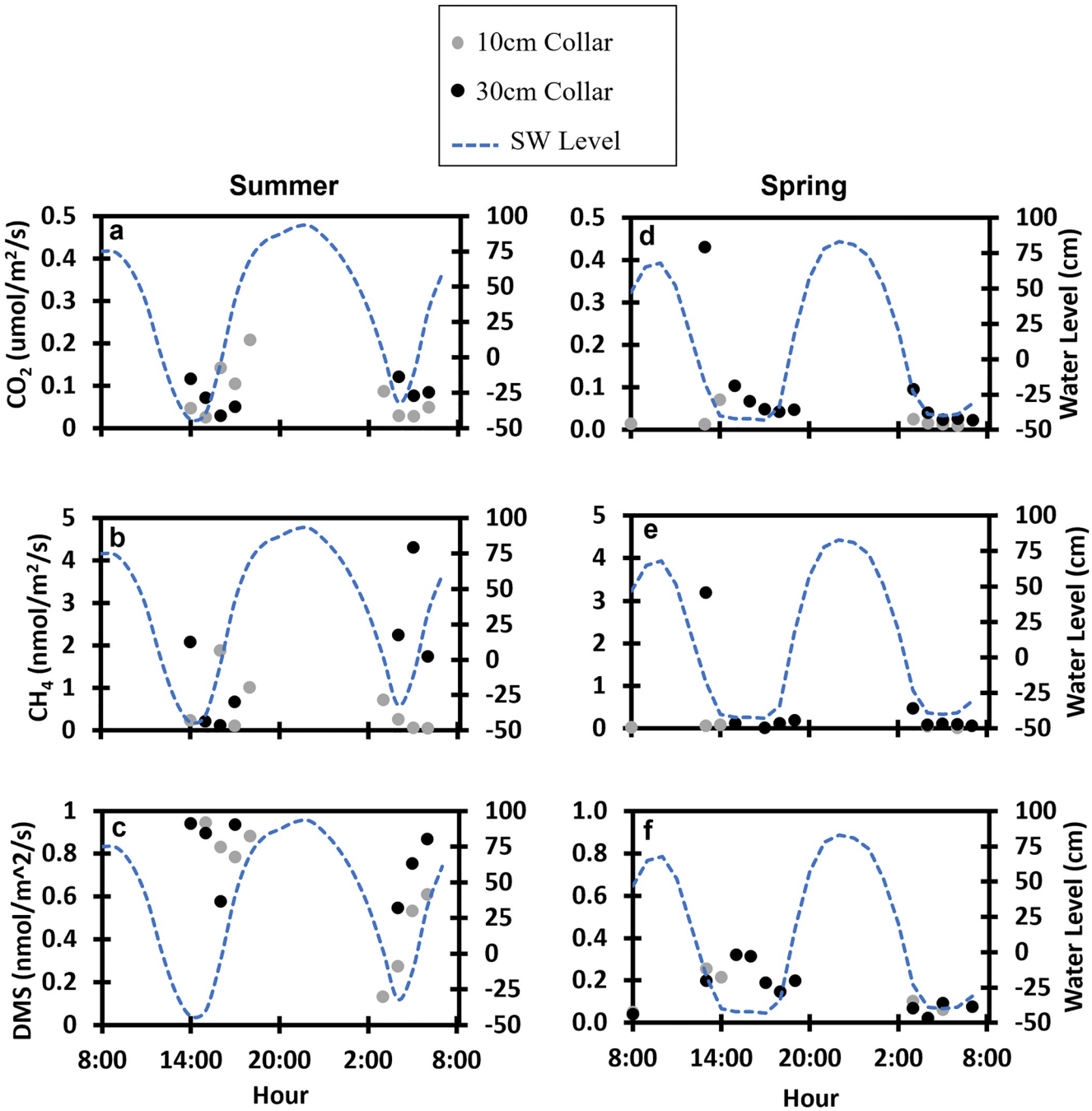

Figure 7. Plots of soil gas (CO_2, CH_4, DMS) fluxes with tidal channel surface water (SW) oscillation. Plots (a–c) are from the summer, while panels (d–f) are from the spring. Fluxes are represented as points instead of lines due to being unable to sample across the entire tidal cycle since the flux collars were underwater at higher tidal stages.

of C in the tidal channel and the direction and magnitude of solute flow driven by the hydraulic gradient. In the spring, DOC, DIC, and Fe^{2+} were significantly higher in the tidal channel when the hydraulic gradient drove flow toward the channel (Table 4b). Our porewater data show that the groundwater is a substantial source of these solutes. In addition, tidal channel solute concentrations, including both DOC and DIC, increased as the hydraulic gradient increased, consistent with an increased flux of solute-rich groundwater/porewater to the channel. Groundwater flowing into the tidal channel during positive gradients increases CDOM in the surface water. Our EEMs UV-VIS data support this interpretation as Coble A and C peaks were twice as high in the channel during

Version of Record at: https://doi.org/10.1029/2023JG007404

periods of positive gradients compared to negative gradients and correlated significantly with the hydraulic gradient ($R^2 = 0.50$, $R^2 = 0.50$). While positive gradients increased channel solutes, including C, that had more of a terrestrial CDOM signature, negative gradients led to an increase of marine-like C in the tidal channel.

Periods of negative gradients corresponded with periods when surface water was significantly saltier and higher in Sr and BIX intensities than periods of positive gradients. Therefore, water infiltrating the marsh platform when the flow is driven into the channel bank soils has more of a marine component. While the marine signatures (i.e., higher BIX, higher S_r) are more intense during negative gradients, terrestrial signatures (i.e., HIX, Coble Peaks) are still appreciable during these periods. Therefore, the tidal channel is a mixture of allochthonous marine-derived C and autochthonous marsh-derived C, but the relative contributions of each source (marine vs. terrestrial) change with tidal oscillation.

While the spring channel solutes showed clear differences and relationships with the hydraulic gradient, the summer data set did not. Porewater solute concentrations in the tidal channel did not form significant relationships with hydraulic gradient and were not significantly different between positive and negative gradients, nor were the characterization properties (Coble A & C, S_r, BIX) (Table 4a). While the hydraulic gradient in the summer was similar in range to the spring, the groundwater level rarely dropped below the soil surface. This indicates that although the sampling events occurred on the same tidal cycle event (i.e., spring tide), the hydrologic processes involved in horizontal exchange likely differed. In the summer, higher high tides caused overtopping of the bank soils and overland flow, causing the marsh platform to remain fully saturated with flooded conditions above it, even as the channel receded, taking much longer to drain than in the spring. In the overtopping case, groundwater would flow into the channel during the ebb and low tide, driven by the flooded conditions and higher groundwater heads, but would be replenished by vertical infiltration of floodwater into the marsh sediments. Thus, a more expansive zone of groundwater adjacent to the channel would be flushed with channel water, reducing the influence of groundwater discharge on channel water quality due to similar solute concentrations. This could explain the weaker relationships between hydraulic gradient and tidal channel solutes in the summer because the horizontal exchange would be composed of higher amounts of infiltrated channel water rather than porewater-derived solutes. This could be another source of uncertainty because lateral C fluxes may differ even during the same tidal events.

Based on discharge values from the marsh platform to the tidal channel calculated from a previous study at the field site (Guiimond, Yu, et al., 2020; Guimond, Seyfferth, et al., 2020) and the average porewater concentrations during gradients driving flow toward the channel in this study, we estimate per meter of tidal channel that 0.12 ± 0.03 g DOC day^{-1} and 0.31 ± 0.11 g DIC day^{-1} are horizontally exported into the tidal channel in the summer, while 0.01 ± 0.002 g DOC day^{-1} and 0.02 ± 0.004 g DIC day^{-1} are horizontally exported into the tidal channel in the spring. Differences in flux rates could be attributed to seasonal C concentrations and hydraulic conductivity differences between summer and spring, partially driven by crab burrow activity (Guiimond, Yu, et al., 2020; Guimond, Seyfferth, et al., 2020) and plant activity (Trifunovic et al., 2020). These findings indicate that the horizontal exchange of solutes at the marsh-tidal channel interface drives variability in lateral C flux. Furthermore, porewater DIC contributes ~2x more to horizontal C export than porewater DOC in both seasons, but seasonal variability in both DOC and DIC export can vary by ~10x as shown in this study.

4.4. Trace Gas Fluxes From the Channel Bank Are Influenced by Groundwater Oscillations

Lateral C fluxes tended to focus on particulate and dissolved C, often leaving out the assessment of trace gas fluxes which ultimately decrease the global cooling effect of stored C in coastal ecosystems (Santos et al., 2019). Trace gas fluxes from tidal channels may exceed vertical soil fluxes and require more attention because the mechanisms controlling emissions near channel banks are not fully understood (Trifunovic et al., 2020). We hypothesized that fluxes of horizontal gases from the channel bank are partially controlled by the rising and falling tides, whereby rising groundwater pushes gases up and outward from the channel bank. We found that several soil gases (CO_2, CH_4, DMS) were emitted from the channel bank and positively correlated with groundwater oscillation during certain tidal stages. DMS was strongly related to groundwater levels, suggesting a strong physical control of groundwater mainly during the spring at the 10 cm collar ($R^2 = 0.52$), but it is known that the temporal variability of this trace gas could be very large (Capooci & Vargas, 2022b). Soil CO_2 fluxes also had an apparent positive relationship with groundwater level at 30 cm collar in the summer ($R^2 = 0.51$). These findings indicate that the movement of soil trace gases out of the channel bank with tides can be incorporated into future

Version of Record at: https://doi.org/10.1029/2023JG007404

modeling efforts, although long-term (e.g., seasonal) patterns are likely a combination of hydrological patterns, temperature dependence, and phenological stages of the ecosystem (Vázquez-Lule & Vargas, 2021).

We identify several challenges to improve our understanding of trace gas fluxes in terrestrial-aquatic interfaces across the marsh platform and adjacent creeks. First, this study quantified trace gas fluxes from creek bank soils/sediments exposed to the atmosphere during low tides, but it is unknown the rate of gas (and other mass) exchange when the sediments are submerged during high tides. Second, spatial variability across the terrestrial-aquatic interface of the marsh platform and adjacent creeks should be better represented by combining information from different topographic positions (e.g., high-, low-marsh, channel banks) and water-atmosphere fluxes. Third, future studies should consider implementing long-term automated measurements of diverse trace gas fluxes to identify patterns and controls at multiple temporal scales (Capooci & Vargas, 2022b). Finally, the appropriate measurements in time and space of trace gas fluxes constitute a science frontier when reporting carbon budgets and assessments of nature-based solutions (Vargas & Le, 2023).

5. Conclusion

The lateral C fluxes in tidal salt marshes may account for a substantial fraction of the net C flux, though current estimates remain highly variable. We propose several mechanisms that control the exchange of horizontal C between the tidal channel surface water and soil porewater interface that may help understand sources of variation in lateral C flux. First, our porewater data show evidence of tidally driven chemical processes in which Fe oxides immobilize DOC during ebb tides that oxgenate soils and remobilize DOC during flood tide. Second, the concentration and source of C found in the tidal channel changed based on the hydraulic gradient (i.e., flow direction) between the tidal channel and the marsh platform. Third, CO_2, CH_4, and DMS have substantial horizontal fluxes from the channel bank, and fluxes tend to increase with rising groundwater. These physicochemical processes show the importance of considering the horizontal transport of C on small spatial scales to better constrain large-scale lateral C budgets. The mechanisms highlighted here may help to improve and inform biogeochemical lateral C flux models. Future studies should couple solid-phase analysis with porewater and surface water and explore tidal cycles across seasons (e.g., senescence, dormancy) to further examine important horizontal C flux mechanisms and across multiple tidal cycles within each season.

Conflict of Interest

The authors declare no conflicts of interest relevant to this study.

Data Availability Statement

The data set used for this study, Fettrow (2023), is available on Figshare (DOI: https://doi.org/10.6084/m9.figshare.21931932.v1).

Acknowledgments
We thank UD Soil Testing Laboratory for analytical assistance and the staff of the Delaware National Estuarine Research Reserve (DNERR). S.F. acknowledges support from the Delaware Environmental Institute. R.V. acknowledges support from the National Science Foundation (Grant 1652594). A.L.S. and H.M. acknowledge support from the National Science Foundation (Grants 1759879 and 2012484). The authors acknowledge that the land on which they conducted this study is the traditional home of the Lenni-Lenape tribal nation (Delaware nation).

References

Abdul-Aziz, O. I., Ishtiaq, K. S., Tang, J., Moseman-Valtierra, S., Kroeger, K. D., Gonneea, M. E., et al. (2018). Environmental controls, emergent scaling, and predictions of greenhouse gas (GHG) fluxes in coastal salt marshes. *Journal of Geophysical Research: Biogeosciences*, *123*(7), 2234–2256. https://doi.org/10.1029/2018JG004556

Adhikari, D., Sowers, T., Stuckey, J. W., Wang, X., Sparks, D. L., & Yang, Y. (2019). Formation and redox reactivity of ferrihydrite-organic carbon-calcium co-precipitates. *Geochimica et Cosmochimica Acta*, *244*, 86–98. https://doi.org/10.1016/j.gca.2018.09.026

Baker, A., Bolton, L., Newson, M., & Spencer, R. G. M. (2008). Spectrophotometric properties of surface water dissolved organic matter in an afforested upland peat catchment. *Hydrological Processes*, *22*(13), 2325–2336. https://doi.org/10.1002/hyp.6827

Berthelin, J., Laba, M., Lemaire, G., Powlson, D., Tessier, D., Wander, M., & Baveye, P. C. (2022). Soil carbon sequestration for climate change mitigation: Mineralization kinetics of organic inputs as an overlooked limitation. *European Journal of Soil Science*, *73*(1). https://doi.org/10.1111/ejss.13221

Bogard, M. J., Bergamaschi, B. A., Butman, D. E., Anderson, F., Knox, S. H., & Windham-Myers, L. (2020). Hydrologic export is a major component of coastal wetland carbon budgets. *Global Biogeochemical Cycles*, *34*(8), 1–14. https://doi.org/10.1029/2019GB006430

Capooci, M., Barba, J., Seyfferth, A. L., & Vargas, R. (2019). Experimental influence of storm-surge salinity on soil greenhouse gas emissions from a tidal salt marsh. *Science of the Total Environment*, *686*, 1164–1172. https://doi.org/10.1016/j.scitotenv.2019.06.032

Capooci, M., & Vargas, R. (2022a). Diel and seasonal patterns of soil CO_2 efflux in a temperate tidal marsh. *Science of the Total Environment*, *802*, 149715. https://doi.org/10.1016/j.scitotenv.2021.149715

Capooci, M., & Vargas, R. (2022b). Trace gas fluxes from tidal salt marsh soils: Implications for carbon–sulfur biogeochemistry. *Biogeosciences*, *19*, 4655–4670. https://doi.org/10.5194/bg-19-4655-2022

Version of Record at: https://doi.org/10.1029/2023JG007404

Charlson, R. J., Lovelock, J. E., Andreae, M. O., & Warren, S. G. (1987). Oceanic phytoplankton, atmospheric sulphur, cloud albedo and climate. *Nature*, *326*(6114), 655–661. https://doi.org/10.1038/326655a0

Chen, C., Dynes, J. J., Wang, J., & Sparks, D. L. (2014). Properties of Fe-organic matter associations via coprecipitation versus adsorption. *Environmental Science and Technology*, *48*(23), 13751–13759. https://doi.org/10.1021/es503669u

Chen, C., & Sparks, D. L. (2015). Multi-elemental scanning transmission X-ray microscopy-near edge X-ray absorption fine structure spectroscopy assessment of organo-mineral associations in soils from reduced environments. *Environmental Chemistry*, *12*(1), 64–73. https://doi.org/10.1071/EN14042

Chmura, G. L., Anisfeld, S. C., Cahoon, D. R., & Lynch, J. C. (2003). Global carbon sequestration in tidal, saline wetland soils. *Global Biogeochemical Cycles*, *17*(4), 1111. https://doi.org/10.1029/2002GB001917

Chu, S. N., Wang, Z. A., Gonneea, M. E., Kroeger, K. D., & Ganju, N. K. (2018). Deciphering the dynamics of inorganic carbon export from intertidal salt marshes using high-frequency measurements. *Marine Chemistry*, *206*(August), 7–18. https://doi.org/10.1016/j.marchem.2018.08.005

Cline, J. D. (1969). Spectrophotometric determination of hydrogen sulfide in natural waters. *Limnology & Oceanography*, *14*(3), 454–458. https://doi.org/10.4319/lo.1969.14.3.0454

Cory, R. M., McNeill, K., Cotner, J. P., Amado, A., Purcell, J. M., & Marshall, A. G. (2010). Singlet oxygen in the coupled photochemical and biochemical oxidation of dissolved organic matter. *Environmental Science and Technology*, *44*(10), 3683–3689. https://doi.org/10.1021/es902989y

Czapla, K. M., Anderson, I. C., & Currin, C. A. (2020). Net ecosystem carbon balance in a North Carolina, USA, salt marsh. *Journal of Geophysical Research: Biogeosciences*, *125*(10), 1–16. https://doi.org/10.1029/2019JG005509

Diefenderfer, H. L., Cullinan, V. I., Borde, A. B., Gunn, C. M., & Thom, R. M. (2018). High-frequency greenhouse gas flux measurement system detects winter storm surge effects on salt marsh. *Global Change Biology*, *24*(12), 5961–5971. https://doi.org/10.1111/gcb.14430

Duarte, C. M. (2017). Reviews and syntheses: Hidden forests, the role of vegetated coastal habitats in the ocean carbon budget. *Biogeosciences*, *14*(2), 301–310. https://doi.org/10.5194/bg-14-301-2017

Duarte, C. M., Dennison, W. C., Orth, R. J. W., & Carruthers, T. J. B. (2008). The charisma of coastal ecosystems: Addressing the imbalance. *Estuaries and Coasts*, *31*(2), 233–238. https://doi.org/10.1007/s12237-008-9038-7

Duarte, C. M., Losada, I. J., Hendriks, I. E., Mazarrasa, I., & Marbà, N. (2013). The role of coastal plant communities for climate change mitigation and adaptation. *Nature Climate Change*, *3*(11), 961–968. https://doi.org/10.1038/nclimate1970

Fettrow, S. (2023). AGU_TidalCreekPaper_Data.xlsx. figshare. [Dataset]. https://doi.org/10.6084/m9.figshare.21931932.v1

Fettrow, S., Vargas, R., & Seyfferth, A. L. (2023). Experimentally simulated sea level rise destabilizes carbon-mineral associations in temperate tidal marsh soil. *Biogeochemistry*, *163*(2), 103–120. https://doi.org/10.1007/s10533-023-01024-z

Gorham, C., Lavery, P., Kelleway, J. J., Salinas, C., & Serrano, O. (2021). Soil carbon stocks vary across geomorphic settings in Australian temperate tidal marsh ecosystems. *Ecosystems*, *24*(2), 319–334. https://doi.org/10.1007/s10021-020-00520-9

Guimond, J. A., Seyfferth, A. L., Moffett, K. B., & Michael, H. A. (2020). A physical-biogeochemical mechanism for negative feedback between marsh crabs and carbon storage. *Environmental Research Letters*, *15*(3), 034024. https://doi.org/10.1088/1748-9326/ab60e2

Guimond, J. A., Yu, X., Seyfferth, A. L., & Michael, H. A. (2020). Using hydrological-biogeochemical linkages to elucidate carbon dynamics in coastal marshes subject to relative sea level rise. *Water Resources Research*, *56*(2), 1–16. https://doi.org/10.1029/2019WR026302

Hagedorn, F., Kaiser, K., Feyen, H., & Schleppi, P. (2000). Effects of redox conditions and flow processes on the mobility of dissolved organic carbon and nitrogen in a forest soil. *Journal of Environmental Quality*, *29*(1), 288–297. https://doi.org/10.2134/jeq2000.00472425002900010036x

Hayes, D. J., Vargas, R., Alin, S., Conant, R. T., Hutyra, L. R., Jacobson, A. R., et al. (2018). The North American carbon budget. Second state of the carbon cycle report. Second state of the carbon cycle report (SOCCR2): A sustained assessment report.

Helms, J. R., Stubbins, A., Ritchie, J. D., Minor, E. C., Kieber, D. J., & Mopper, K. (2008). Absorption spectral slopes and slope ratios as indicators of molecular weight, source, and photobleaching of chromophoric dissolved organic matter. *Limnology & Oceanography*, *53*(3), 955–969. https://doi.org/10.4319/lo.2008.53.3.0955

Hill, A. C., Vázquez-Lule, A., & Vargas, R. (2021). Linking vegetation spectral reflectance with ecosystem carbon phenology in a temperate salt marsh. *Agricultural and Forest Meteorology*, *307*, 108481. https://doi.org/10.1016/j.agrformet.2021.108481

Hinson, A. L., Feagin, R. A., Eriksson, M., Najjar, R. G., Herrmann, M., Bianchi, T. S., et al. (2017). The spatial distribution of soil organic carbon in tidal wetland soils of the continental United States. *Global Change Biology*, *23*(12), 5468–5480. https://doi.org/10.1111/gcb.13811

Howard, J., Sutton-Grier, A., Herr, D., Kleypas, J., Landis, E., Mcleod, E., et al. (2017). Clarifying the role of coastal and marine systems in climate mitigation. *Frontiers in Ecology and the Environment*, *15*(1), 42–50. https://doi.org/10.1002/fee.1451

Huguet, A., Vacher, L., Relexans, S., Saubusse, S., Froidefond, J. M., & Parlanti, E. (2009). Organic geochemistry properties of fluorescent dissolved organic matter in the Gironde Estuary. *Organic Geochemistry*, *40*(6), 706–719. https://doi.org/10.1016/j.orggeochem.2009.03.002

IPCC. (2014). Summary for policymakers. In *World in transition 3* (pp. 23–32). Routledge. https://doi.org/10.4324/9781315071961-11

Keene, A., Johnston, S., Bush, R., Sullivan, L., & Burton, E. (2010). *Reductive dissolution of natural jarosite in a tidally inundated acid sulfate soil: Geochemical implications*. World Congress of Soil Science.

Limmer, M. A., Mann, J., Amaral, D. C., Vargas, R., & Seyfferth, A. L. (2018). Silicon-rich amendments in rice paddies: Effects on arsenic uptake and biogeochemistry. *Science of the Total Environment*, *624*, 1360–1368. https://doi.org/10.1016/j.scitotenv.2017.12.207

Macreadie, P. I., Costa, M. D. P., Atwood, T. B., Friess, D. A., Kelleway, J. J., Kennedy, H., et al. (2021). Blue carbon as a natural climate solution. *Nature Reviews Earth & Environment*, *2*(12), 826–839. https://doi.org/10.1038/s43017-021-00224-1

Mcleod, E., Chmura, G. L., Bouillon, S., Salm, R., Björk, M., Duarte, C. M., et al. (2016). A blueprint for blue carbon: Toward an improved understanding of the role of vegetated coastal habitats in sequestering CO_2. *Frontiers in Ecology and the Environment*, *9*(10), 552–560. https://doi.org/10.1890/110004

Najjar, R. G., Herrmann, M., Alexander, R., Boyer, E. W., Burdige, D. J., Butman, D., et al. (2018). Carbon budget of tidal wetlands, estuaries, and shelf waters of eastern North America. *Global Biogeochemical Cycles*, *32*(3), 389–416. https://doi.org/10.1002/2017GB005790

Nellemann, C., Corcoran, E., Duarte, C. M., Valdés, L., de Young, C., Fonseca, L., & Grimsditch, G. (2009). Blue carbon - the role of healthy oceans in binding carbon. Retrieved from https://wedocs.unep.org/handle/20.500.11822/7772

Northrup, K., Capooci, M., & Seyfferth, A. L. (2018). Effects of extreme events on arsenic cycling in salt marshes. *Journal of Geophysical Research: Biogeosciences*, *123*(3), 1086–1100. https://doi.org/10.1002/2017JG004259

O'Connor, J. J., Fest, B. J., Sievers, M., & Swearer, S. E. (2020). Impacts of land management practices on blue carbon stocks and greenhouse gas fluxes in coastal ecosystems—A meta-analysis. *Global Change Biology*, *26*(3), 1354–1366. https://doi.org/10.1111/gcb.14946

Osburn, C. L., Mikan, M. P., Etheridge, J. R., Burchell, M. R., & Birgand, F. (2015). Seasonal variation in the quality of dissolved and particulate organic matter exchanged between a salt marsh and its adjacent estuary. *Journal of Geophysical Research G: Biogeosciences*, *120*(7), 1430–1449. https://doi.org/10.1002/2014JG002897

Version of Record at: https://doi.org/10.1029/2023JG007404

Parrello, D., Zegeye, A., Mustin, C., & Billard, P. (2016). Siderophore-mediated iron dissolution from nontronites is controlled by mineral crystallochemistry. *Frontiers in Microbiology*, *7*(MAR). https://doi.org/10.3389/fmicb.2016.00423

Pearson, A. J., Pizzuto, J. E., & Vargas, R. (2016). Influence of run of river dams on floodplain sediments and carbon dynamics. *Geoderma*, *272*, 51–63. https://doi.org/10.1016/j.geoderma.2016.02.029

Petrakis, S., Seyfferth, A., Kan, J., Inamdar, S., & Vargas, R. (2017). Influence of experimental extreme water pulses on greenhouse gas emissions from soils. *Biogeochemistry*, *133*(2), 147–164. https://doi.org/10.1007/s10533-017-0320-2

Pohl, L., Kölbl, A., Uteau, D., Peth, S., Häusler, W., Mosley, L., et al. (2021). Porosity and organic matter distribution in jarositic phyto tubules of sulfuric soils assessed by combined μCT and NanoSIMS analysis. *Geoderma*, *399*, 115124. https://doi.org/10.1016/j.geoderma.2021.115124

Riedel, T., Zak, D., Biester, H., & Dittmar, T. (2013). Iron traps terrestrially derived dissolved organic matter at redox interfaces. *Proceedings of the National Academy of Sciences*, *110*(25), 10101–10105. https://doi.org/10.1073/pnas.1221487110

Santos, I. R., Burdige, D. J., Jennerjahn, T. C., Bouillon, S., Cabral, A., Serrano, O., et al. (2021). The renaissance of Odum's outwelling hypothesis in "Blue Carbon" science. *Estuarine, Coastal and Shelf Science*, *255*(April), 107361. https://doi.org/10.1016/j.ecss.2021.107361

Santos, I. R., Maher, D. T., Larkin, R., Webb, J. R., & Sanders, C. J. (2019). Carbon outwelling and outgassing vs. burial in an estuarine tidal channel surrounded by mangrove and saltmarsh wetlands. *Limnology & Oceanography*, *64*(3), 996–1013. https://doi.org/10.1002/lno.11090

Schwertmann, U. (1991). Solubility and dissolution of iron oxides. *Plant and Soil*, *130*(1), 1–25. https://doi.org/10.1007/bf00011851

Serrano, O., Lovelock, C. E., Atwood, B. T., Macreadie, P. I., Canto, R., Phinn, S., et al. (2019). Australian vegetated coastal ecosystems as global hotspots for climate change mitigation. *Nature Communications*, *10*(1), 4313. https://doi.org/10.1038/s41467-019-12176-8

Seyfferth, A. L., Bothfeld, F., Vargas, R., Stuckey, J. W., Wang, J., Kearns, K., et al. (2020). Spatial and temporal heterogeneity of geochemical controls on carbon cycling in a tidal salt marsh. *Geochimica et Cosmochimica Acta*, *282*, 1–18. https://doi.org/10.1016/j.gca.2020.05.013

Sodano, M., Lerda, C., Nisticò, R., Martin, M., Magnacca, G., Celi, L., & Said-Pullicino, D. (2017). Dissolved organic carbon retention by coprecipitation during the oxidation of ferrous iron. *Geoderma*, *307*(June), 19–29. https://doi.org/10.1016/j.geoderma.2017.07.022

Sowers, T. D., Adhikari, D., Wang, J., Yang, Y., & Sparks, D. L. (2018). Spatial associations and chemical composition of organic carbon sequestered in Fe, Ca, and organic carbon ternary systems. *Environmental Science and Technology*, *52*(12), 6936–6944. https://doi.org/10.1021/acs.est.8b01158

Sowers, T. D., Holden, K. L., Coward, E. K., & Sparks, D. L. (2019). Dissolved organic matter sorption and molecular fractionation by naturally occurring bacteriogenic iron (Oxyhydr)oxides. *Environmental Science and Technology*, *53*(8), 4295–4304. https://doi.org/10.1021/acs.est.9b00540

Sowers, T. D., Stuckey, J. W., & Sparks, D. L. (2018). The synergistic effect of calcium on organic carbon sequestration to ferrihydrite. *Geochemical Transactions*, *19*(1), 22–26. https://doi.org/10.1186/s12932-018-0049-4

Spivak, A. C., Sanderman, J., Bowen, J. L., Canuel, E. A., & Hopkinson, C. S. (2019). Global-change controls on soil-carbon accumulation and loss in coastal vegetated ecosystems. *Nature Geoscience*, *12*(9), 685–692. https://doi.org/10.1038/s41561-019-0435-2

Stookey, L. L. (1970). Ferrozine-A new spectrophotometric reagent for iron. *Analytical Chemistry*, *42*(7), 779–781. https://doi.org/10.1021/ac60289a016

Sun, H., Jiang, J., Cui, L., Feng, W., Wang, Y., & Zhang, J. (2019). Soil organic carbon stabilization mechanisms in a subtropical mangrove and salt marsh ecosystems. *Science of the Total Environment*, *673*, 502–510. https://doi.org/10.1016/j.scitotenv.2019.04.122

Tong, C., Luo, M., Huang, J., She, C., Li, Y., & Ren, P. (2020). Greenhouse gas fluxes and porewater geochemistry following short-term pulses of saltwater and Fe(III) in a subtropical tidal freshwater estuarine marsh. *Geoderma*, *369*(March), 114340. https://doi.org/10.1016/j.geoderma.2020.114340

Trifunovic, B., Vázquez-Lule, A., Capooci, M., Seyfferth, A. L., Moffat, C., & Vargas, R. (2020). Carbon dioxide and methane emissions from A temperate salt marsh tidal channel. *Journal of Geophysical Research: Biogeosciences*, *125*(8). https://doi.org/10.1029/2019JG005558

Tzortziou, M., Neale, P. J., Osburn, C. L., Megonigal, J. P., Maie, N., & Jaffé, R. (2008). Tidal marshes as a source of optically and chemically distinctive colored dissolved organic matter in the Chesapeake Bay. *Limnology & Oceanography*, *53*(1), 148–159. https://doi.org/10.4319/lo.2008.53.1.0148

Van De Broek, M., Temmerman, S., Merckx, R., & Govers, G. (2016). Controls on soil organic carbon stocks in tidal marshes along an estuarine salinity gradient. *Biogeosciences*, *13*(24), 6611–6624. https://doi.org/10.5194/bg-13-6611-2016

Vargas, R., & Le, V. H. (2023). The paradox of assessing greenhouse gases from soils for nature-based solutions. *Biogeosciences*, *20*(1), 15–26. https://doi.org/10.5194/bg-20-15-2023

Vázquez-Lule, A., & Vargas, R. (2021). Biophysical drivers of net ecosystem and methane exchange across phenological phases in a tidal salt marsh. *Agricultural and Forest Meteorology*, *300*, 108309. https://doi.org/10.1016/j.agrformet.2020.108309

Wang, J., & Wang, J. (2017). *Spartina alterniflora* alters ecosystem DMS and CH_4 emissions and their relationship along interacting tidal and vegetation gradients within a coastal salt marsh in Eastern China. *Atmospheric Environment*, *167*, 346–359. https://doi.org/10.1016/j.atmosenv.2017.08.041

Wang, Z. A., & Cai, W. (2004). Carbon dioxide degassing and inorganic carbon export from a marsh-dominated estuary (the Duplin River): A marsh CO_2 pump. *Limnology & Oceanography*, *49*(2), 341–354. https://doi.org/10.4319/lo.2004.49.2.0341

Wang, Z. A., Kroeger, K. D., Ganju, N. K., Gonneea, M. E., & Chu, S. N. (2016). Intertidal salt marshes as an important source of inorganic carbon to the coastal ocean. *Limnology & Oceanography*, *61*(5), 1916–1931. https://doi.org/10.1002/lno.10347

Winter, P. E. D., Schlacher, T. A., & Baird, D. (1996). Carbon flux between an estuary and the ocean: A case for outwelling. *Hydrobiologia*, *337*(1–3), 123–132. https://doi.org/10.1007/BF00028513

Wollenberg, J. T., Biswas, A., & Chmura, G. L. (2018). Greenhouse gas flux with reflooding of a drained salt marsh soil. *PeerJ*, *2018*(11), 1–21. https://doi.org/10.7717/peerj.5659

Wordofa, D. N., Adhikari, D., Dunham-Cheatham, S. M., Zhao, Q., Poulson, S. R., Tang, Y., & Yang, Y. (2019). Biogeochemical fate of ferrihydrite-model organic compound complexes during anaerobic microbial reduction. *Science of the Total Environment*, *668*, 216–223. https://doi.org/10.1016/j.scitotenv.2019.02.441

Xin, P., Yuan, L.-R., Li, L., & Barry, D. A. (2011). Tidally driven multiscale pore water flow in a channel-marsh system. *Water Resources Research*, *47*(7). https://doi.org/10.1029/2010WR010110

Yu, C., Xie, S., Song, Z., Xia, S., & Åström, M. E. (2021). Biogeochemical cycling of iron (hydr-)oxides and its impact on organic carbon turnover in coastal wetlands: A global synthesis and perspective. *Earth Science Reviews*, *218*, 103658. https://doi.org/10.1016/j.earscirev.2021.103658

Yu, J., Dong, H., Li, Y., Wu, H., Guan, B., Gao, Y., et al. (2014). Spatiotemporal distribution characteristics of soil organic carbon in newborn coastal wetlands of the Yellow River delta estuary. *Clean - Soil, Air, Water*, *42*(3), 311–318. https://doi.org/10.1002/clen.201100511

Version of Record at: https://doi.org/10.1029/2023JG007404

Zak, D., & Gelbrecht, J. (2007). The mobilisation of phosphorus, organic carbon and ammonium in the initial stage of fen rewetting (a case study from NE Germany). *Biogeochemistry*, *85*(2), 141–151. https://doi.org/10.1007/s10533-007-9122-2

Zhang, Q., Yan, Z., & Li, X. (2021). Iron plaque formation and rhizosphere iron bacteria in *Spartina alterniflora* and *Phragmites australis* on the redoxcline of tidal flat in the Yangtze River estuary. *Geoderma*, *392*, 115000. https://doi.org/10.1016/j.geoderma.2021.115000